Scaling of fracture systems in geological media

SCALING OF FRACTURE SYSTEMS IN GEOLOGICAL MEDIA

E. Bonnet,[1] O. Bour,[2] N. E. Odling,[1,3] P. Davy,[2]
I. Main,[4] P. Cowie,[4] and B. Berkowitz[5]

Abstract. Scaling in fracture systems has become an active field of research in the last 25 years motivated by practical applications in hazardous waste disposal, hydrocarbon reservoir management, and earthquake hazard assessment. Relevant publications are therefore spread widely through the literature. Although it is recognized that some fracture systems are best described by scale-limited laws (lognormal, exponential), it is now recognized that power laws and fractal geometry provide widely applicable descriptive tools for fracture system characterization. A key argument for power law and fractal scaling is the absence of characteristic length scales in the fracture growth process. All power law and fractal characteristics in nature must have upper and lower bounds. This topic has been largely neglected, but recent studies emphasize the importance of layering on all scales in limiting the scaling characteristics of natural fracture systems. The determination of power law exponents and fractal dimensions from observations, although outwardly simple, is problematic, and uncritical use of analysis techniques has resulted in inaccurate and even meaningless exponents. We review these techniques and suggest guidelines for the accurate and objective estimation of exponents and fractal dimensions. Syntheses of length, displacement, aperture power law exponents, and fractal dimensions are found, after critical appraisal of published studies, to show a wide variation, frequently spanning the theoretically possible range. Extrapolations from one dimension to two and from two dimensions to three are found to be nontrivial, and simple laws must be used with caution. Directions for future research include improved techniques for gathering data sets over great scale ranges and more rigorous application of existing analysis methods. More data are needed on joints and veins to illuminate the differences between different fracture modes. The physical causes of power law scaling and variation in exponents and fractal dimensions are still poorly understood.

1. INTRODUCTION

The study of *fracture* systems (terms in italic are defined in the glossary, after the main text) has been an active area of research for the last 25 years motivated to a large extent by the siting of hazardous waste disposal sites in crystalline rocks, by the problems of multiphase flow in fractured hydrocarbon reservoirs, and by earthquake hazards and the possibility of prediction. Here we define a fracture as any discontinuity within a rock mass that developed as a response to stress. This comprises primarily mode I and mode II fractures. In mode I fracturing, fractures are in tensile or opening mode in which displacements are normal to the discontinuity walls (*joints* and many *veins*). *Faults* correspond to mode II fractures, i.e., an in-plane shear mode, in which the displacements are in the plane of the discontinuity. Fractures exist on a wide range of scales from microns to hundreds of kilometers, and it is known that throughout this scale range they have a significant effect on processes in the Earth's crust including fluid flow and rock strength.

Early work was spread though a wide range of scales from core through *outcrop* to aerial photographs and satellite image scales. More recently, the manner in which fracture system properties at different scales relate to each other, i.e., their scaling attributes, has received increasing attention motivated by the promise of statistical prediction that scaling laws offer. In earthquake hazard assessment, the main issue is the validity of the Gutenberg-Richter law for predicting the probability of occurrence of large earthquakes. In the case of the hydrocarbon industry, such scaling laws provide a key to predicting the nature of subseismic fracturing (below the limit of seismic resolution), which can significantly influence reservoir and cap rock quality, from seismically resolved faults. In groundwater applications, contaminant transport is particularly sensitive to the properties and scaling of fracture systems. *Fractal* geometry is in many cases well suited to the description of objects that exhibit scaling behavior. The most important feature of fractal geometry is the lack of any homogenization scale

[1]Nansen Center, Bergen, Norway.
[2]Geosciences Rennes, Université Rennes, Rennes, France.
[3]Now at Rock Deformation Research Group, School of Earth Sciences, University of Leeds, Leeds, England, United Kingdom.
[4]Department of Geology and Geophysics, University of Edinburgh, Edinburgh, Scotland, United Kingdom.
[5]Department of Environmental Sciences and Energy Research, Weizmann Institute of Science, Rehovot, Israel.

Reviews of Geophysics, 39, 3 / *August 2001*
pages 347–383
8755-1209/01/1999RG000074$15.00
Paper number 1999RG000074

or representative elementary volume. This has serious consequences for the use of continuum mechanics for describing the behavior of the lithosphere or the use of equivalent porous media to describe the hydraulic behavior of fractured media, since both require the definition of a homogenization scale.

The numerous studies of fracture system scaling in the literature do indeed suggest that such scaling laws exist in nature. They also indicate, however, that such scaling laws must be used with caution and with due regard to the physical influences that govern their validity. Recent studies indicate that lithological layering from the scale of a single bed to the whole crust is reflected in fracture system properties and influences the scale range over which individual scaling laws are valid. The impact of these scaling laws for processes in the Earth's crust such as fluid flow, rock strength, and seismic hazard is a field that is now beginning to be explored and promises to be an active area of research in the future.

The subject of scaling in fracture systems has received attention from workers in many fields including geology, geophysics, physics, applied mathematics, and engineering. Communication between these different groups, who often employ different terminologies, has not always been optimal. Thus we have included a tutorial that attempts to define and make clear the links between the different types of statistical description that appear in the literature. The relevant literature is spread throughout a wide variety of journals, and here we attempt to pull together information from these different sources. For the sake of brevity we have confined this review to the scaling of fracture systems and have not included the scaling properties of fracture surfaces themselves, for which there is a large volume of literature. In the following, we have focused on the scaling properties of fracture systems related either to their size distributions or to their spatial properties. Fracture size is commonly described by its length, by the tangential or perpendicular displacement associated with the fracture, or by its aperture, which is defined as the distance between the fracture walls. We also outline the physical processes that are responsible for scaling behavior and deal, in some detail, with the practical problems of estimating power law exponents and fractal dimensions.

2. STATISTICAL DESCRIPTION IN FRACTURE CHARACTERIZATION

In recent years the power law distribution has been increasingly employed to describe the frequency distribution of fracture properties and geometry. However, a power law is not an appropriate model in all cases, and other distributions that have been used include the lognormal, gamma, and exponential laws (Figure 1). In the following, a brief description of these distributions $n(w)$ is given, where w refers to the study fracture property (length, displacement, and so forth).

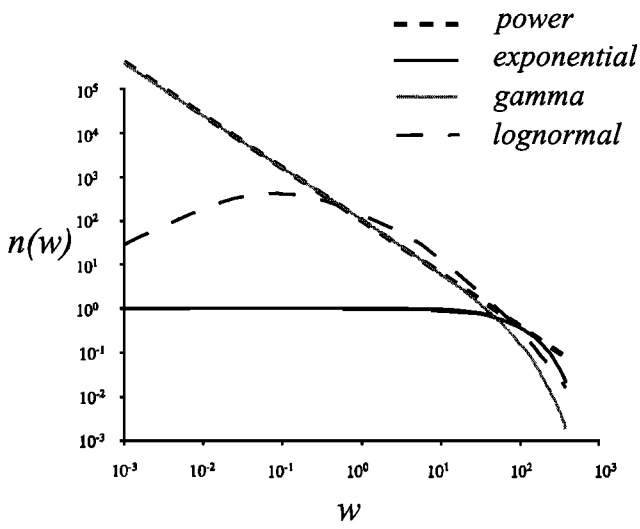

Figure 1. Plot illustrating the four different functions (power, lognormal, exponential, and gamma law) most often used to fit data sets. Data over more than 1 order of magnitude are needed before these different distributions can be easily distinguished.

2.1. Lognormal Distribution

This law has commonly been used to describe fracture length distributions [*Priest and Hudson*, 1981; *Rouleau and Gale*, 1985], and indeed, many raw fracture data sets (trace lengths, fault throws) show an apparently good fit to this distribution. The lognormal distribution is given by

$$n(w) = 1/(w\sigma\sqrt{2\pi}) \exp\left(-\frac{[\log(w) - \langle\log(w)\rangle]^2}{2\sigma^2}\right), \quad (1)$$

where the two parameters $\langle\log(w)\rangle$ and σ are the logarithmic mean and variance, respectively, of the fracture property w (i.e., length, displacement). More recently, however, it has been appreciated that resolution effects (known as truncation) imposed on a power law population can result in a lognormal distribution because fractures with values smaller than the distribution mode are incompletely sampled [*Einstein and Baecher*, 1983; *Segall and Pollard*, 1983]. Thus, with the rise of scaling concepts in Earth sciences, power law distributions have been favored over lognormal distributions because of their greater physical significance [*Barton and Zoback*, 1992]. However, all power laws in nature must have upper and lower cutoffs. The presence of a characteristic length scale in the system provided, for example, by lithological layering, can give rise to lognormal distributions that reflect reality [*Odling et al.*, 1999].

2.2. Exponential Law

This law has been used to describe the size of discontinuities in continental rocks [*Cruden*, 1977; *Hudson and Priest*, 1979, 1983; *Priest and Hudson*, 1981; *Nur*, 1982] and in the vicinity of mid-oceanic ridges [*Carbotte and McDonald*, 1994; *Cowie et al.*, 1993b]. In these cases, fracture growth results from a uniform stress distribution [*Dershowitz and Einstein*, 1988], and propagation of fractures can be compared to a Poisson process [*Cruden*, 1977] resulting in an exponential distribution given by

$$n(w) = A_2 \exp(-w/w_0), \quad (2)$$

where A_2 is a constant. The exponential law incorporates a characteristic scale w_0 (equation (2)) that reflects either a physical length in the system, such as the thickness of a sedimentary layer or the brittle crust [*Cowie*, 1998], or a spontaneous feedback processes during fracture growth [*Renshaw*, 1999]. Numerical simulations performed by *Cowie et al.* [1995] and experimental results of *Bonnet* [1997] have shown that exponential distributions of fracture length are also associated with the early stages of deformation, when fracture nucleation dominates over growth and coalescence processes.

An alternative to the power and exponential laws is the stretched exponential that plays an intermediate role [*Laherrere and Sornette*, 1998]. This law, which incorporates characteristic scales, can account for the observed curvature in distributions and is related to large deviations in multiplicative processes [*Frisch and Sornette*, 1997].

2.3. Gamma Law

The gamma distribution is a power law with an exponential tail and is in common use in fault or earthquake statistics and seismic hazard assessment [*Davy*, 1993; *Main*, 1996; *Kagan*, 1997; *Sornette and Sornette*, 1999]. Any population that obeys this kind of distribution is characterized by a power law exponent a and a characteristic scale w_0 (equation (3)).

$$n(w) = A_3 w^{-a} \exp(-w/w_0). \quad (3)$$

In the physics of critical point phenomena [*Yeomans*, 1992, equation 2.12] the distribution of object size (i.e., length, displacement, aperture) or spacing may take this form. The characteristic scale w_0 may be related to (for example) the correlation length in the spatial pattern, where it implies an upper bound for fractal behavior [*Stauffer and Aharony*, 1994], or may depend on deformation rate [*Main and Burton*, 1984]. When w_0 is greater than the size of the system w_{max}, the gamma law reduces to a power law, and, conversely, a power law with a strong finite size effect (see section 5.1.2) may also resemble a gamma law.

2.4. Power Law

Numerous studies at various scales and in different tectonic settings have shown that the distribution of many fracture properties (i.e., length, displacement) often follows a power law (see sections 6 and 7):

$$n(w) = A_4 w^{-a}. \quad (4)$$

Power law distributions have the important consequence that they contain no characteristic length scale (equation (4)). In nature the power laws have to be limited by physical length scales that form the upper and lower limits to the scale range over which they are valid. It is now generally recognized that resolution and finite size effects on a power law population can also result in distributions that appear to be exponential or lognormal. There appear to be physical grounds for why fracture properties should follow power laws, and these are discussed in section 4. Since power law distributions are playing an increasing role in our understanding of fracture systems, the following sections concentrate largely on this distribution and the estimation of its parameters.

3. DETERMINATION OF POWER LAW EXPONENTS AND FRACTAL DIMENSIONS FOR FRACTURE SYSTEMS: A TUTORIAL

There has been a tendency for workers from different disciplines to use different methods for characterizing power law fracture size distributions and fractal dimensions. The value of the relevant power law exponent or fractal dimension obtained depends on the method used, which has led to some confusion in the literature. For the benefit of those new to this field, the basic methods of determining power law exponents from fracture population size data, and fractal dimensions from fracture spatial data, are briefly reviewed here. Readers already familiar with these methods may wish to skip to section 4.

3.1. Methods for Measuring Size Distributions

A power law may be assumed to be a reasonable model for the size distribution of a fracture population when the distribution trend on a log-log graph shows an acceptable approximation to a straight line over a sufficient scale range. Three different types of distribution are commonly used to characterize fracture size data; these are the frequency, frequency density, and cumulative frequency distributions. In the literature, geologists have most commonly used the cumulative distribution, whereas geophysicists largely use the density distribution because it is more amenable to integration for higher-order moments. The value of the power law exponent depends on the type of distribution on which the analysis is based and also on bin type. Care must be taken to compare like with like for scaling exponents quoted in the literature. In this article we have chosen to use the density distribution as the standard, since the other forms may be easily derived from it. In this tutorial we

TABLE 1. Relationship Between Distributions and Their Exponents

Type of Distribution	*Logarithmic Bin*	*Linear Bin*
Frequency	$a - 1$	a
Density	a	a
Cumulative	$a - 1$	$a - 1$

Comparison between the exponent values for the distributions commonly used for the determination of power law length distributions.

have used fracture trace length l as an illustrative example throughout.

For a population of fractures that follows a power law, the manner in which the number of fractures decreases with size can be described by the frequency distribution

$$N(l) = \alpha l^{-a} dl, \tag{5}$$

where $N(l)$ is the number of fracture lengths that belong to the interval $[l, l + dl]$ for $dl \ll l$, α is a *density constant*, and a is the exponent. Where the bin size is constant, the exponent equals a, but where the bin size follows a logarithmic progression, the power law exponent is $a - 1$, because $d(\ln(l)) = dl/l$ (see Table 1 and Figure 2). This dependence of the exponent on the type of bin is one reason why the density distribution exponent, which is independent of the type of bin used, is preferable. Another advantage of using the density distribution is the nature of the trend of the distribution at large values where the number of elements belonging to the interval can be very small (see section 5.1 for more details). The density distribution $n(l)$ corresponds to the number of fractures $N(l)$ belonging to an interval divided by the bin size dl [*Davy*, 1993]:

$$n(l) = \alpha l^{-a}. \tag{6}$$

As long as dl is small enough, the density distribution is independent of the chosen bin size. The number of faults $N(l)$ gives the frequency distribution as in any standard histogram plot. For a power law population, a log-log plot of $N(l)$ or $n(l)$ versus l shows a straight line, the slope of which gives the exponent of the power law [*Reches*, 1986; *Scholz and Cowie*, 1990]. The choice of the interval dl is critical in the sense that it defines the degree of smoothing of the distribution trend, and a small change in dl can lead to a significant change in the number of fractures N belonging to each interval. *Davy* [1993] has proposed an objective method for determining the size of interval at which $n(l)$ shows the lowest fluctuations.

The cumulative distribution represents the number of fractures whose length is greater than a given length l and corresponds to the integral of the density distribution $n(l)$

$$C(l) = \int_{l}^{l_{\max}} n(l)\, dl, \tag{7}$$

where $l_{\max}$ is the greatest length encountered in the network. Hence if $n(l)$ is a power law characterized by an exponent equal to a (equation (6)), the cumulative distribution will be a power law for $l \ll l_{\max}$ with an

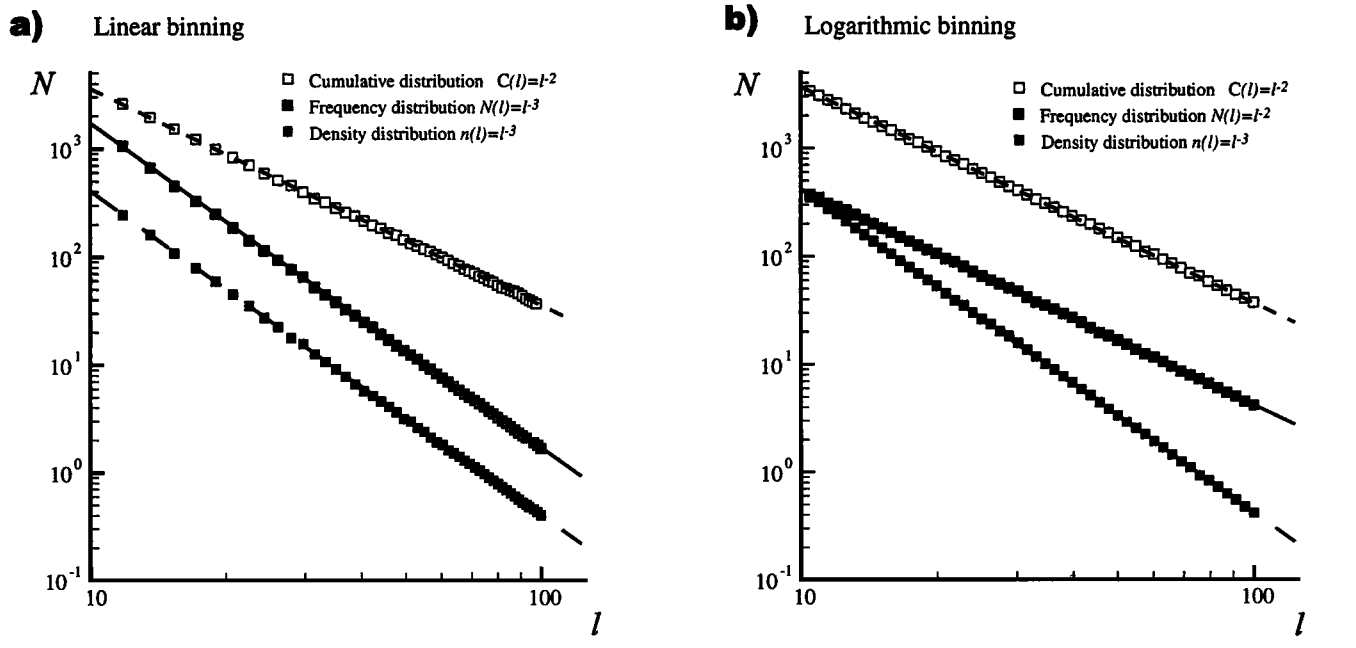

Figure 2. Frequency, density, and cumulative distributions for theoretical population following a power law with a density exponent of 3. Distributions have been calculated for (a) linear binning and (b) logarithmic binning. The exponent changes according to the distribution and type of bin used.

exponent equal to $a - 1$, commonly denoted c [*Childs et al.*, 1990; *Walsh et al.*, 1991; *Jackson and Sanderson*, 1992; *Cowie et al.*, 1993a, 1995; *Pickering et al.*, 1997]. The cumulative distribution has been widely used because it is easily computed and the data do not have to be binned. In practice, it is constructed by summing incremental frequency data, equivalent to introducing a low-pass filter, and hence tends to give a smoother trend than the frequency or density distributions, increasing artificially the regression coefficient. The cumulative distribution is very sensitive to finite size effects, which can make determination of the exponent problematic (see section 5.1). The relationships between the values of the exponents for the frequency, density, and cumulative distributions are compared in Table 1.

All observed fracture populations are affected by "truncation" and "censoring" effects, which alter the appearance of the distribution. Short fractures are incompletely observed as the limit of resolution of the image is approached (truncation), causing a shallowing of slope of the distribution trend at the lower end of the scale range. Long fractures tend to be incompletely sampled because they pass outside the observed region (censoring), causing an artificial steepening of the distribution trend at the upper end of the scale range. A detailed discussion of these effects and the correction methods available is given in section 5.1.

3.2. Methods for Measuring the Fractal Dimension

The mathematical theory of fractals is described by *Mandelbrot* [1982], and more information about fractals is given by *Feder* [1988], *Falconer* [1990], and *Vicsek* [1992]. The fractal dimension does not completely define the geometry of the fracture system, and a complete characterization should include various geometrical attributes such as density, length, orientation, roughness of the fracture surface, width, aperture, shear displacement, and so forth, in addition to the fractal dimension. In the case of fracture systems, two ways of defining the fracture pattern are possible. These are (1) as a fractured domain, where the fracture pattern is considered as a whole, and (2) as a set of fractures, where each fracture defines a separate object. In the latter case the extent of each fracture must be determined, which is then usually characterized by its midpoint (center of mass, or barycenter). Such a definition is particularly convenient for defining the *fracture density*, i.e., the number of fractures per unit area or volume [*Davy et al.*, 1990]. Different methods of determining the fractal dimension are used depending on the quantity measured.

The classical definition of a fractal is given by the number of segments, circles, or spheres of dimension d equal to 1, 2, or 3, and of characteristic length scale r, necessary to cover the part of a fractal object included in volume R^d. This number of circles or spheres should vary as $N(r, R) \approx (R/r)^D$, where D denotes the fractal dimension; $N(r, R)^* r^d$ is an estimate of the length, surface, or volume of the fractal object. According to this definition, D may be defined in two ways:

$$D = \lim_{r \to 0} \frac{\ln N(r)}{\ln (1/r)}, \tag{8}$$

i.e., the typical box-counting method for which the fractal dimension is obtained for infinitely small details of the objects, or

$$D = \lim_{R \to \infty} \frac{\ln N(R)}{\ln (R)}, \tag{9}$$

which is obtained by growing the volume limiting the fractal object. The second method is generally not implemented in a direct way. People generally use the mass method, where the volume of the object is replaced by its mass, which scales as $M(R) \approx R^{D_M}$. D_M is called the *mass dimension*. Since it refers to different geometrical properties of the object, D_M is not necessarily equal to D.

In practice, the mass of the fracture pattern is defined as the total fracture length $L(r)$ included in disks of radius r [*Davy et al.*, 1990; *Sornette et al.*, 1993] (Figure 3a). By averaging over typically 100 disks centered on the fracture pattern, one obtains a function $L(r)$ which should vary with r such that

$$L(r) = r^{D_M}. \tag{10}$$

In the box-counting method, the number of boxes of size r, $N(r)$, required to cover the fractal object is counted (Figure 3b) and should vary as

$$N(r) \approx r^{-D}. \tag{11}$$

Thus, by reporting $N(r)$ versus r in a bilogarithmic plot, the fractal dimension D can be derived as the slope of the straight line. This method has been widely used to measure the fractal dimension of fracture networks [*Okubo and Aki*, 1987; *Barton and Larsen*, 1985; *Barton et al.*, 1986; *Barton and Hsieh*, 1989; *Barton*, 1995a; *Chilès*, 1988]. The box-counting method allows a generalization to the concept of *multifractality* [*Hentschel and Proccacia*, 1983; *Grassberger*, 1983]. The information provided by the box-counting method, which characterizes only the scaling properties of the spatial occupancy of the fracture network, may be complemented by the scaling properties of the fracture densities through the moments of order q. Here the system is first covered by a regular mesh of squares of side length r and the total length $L_i(r)$ of fractures in each square is measured. Then the probability $p_i(r)$ is defined as

$$p_i(r) = \frac{L_i(r)}{\sum_{1}^{n} L_i(r)}, \tag{12}$$

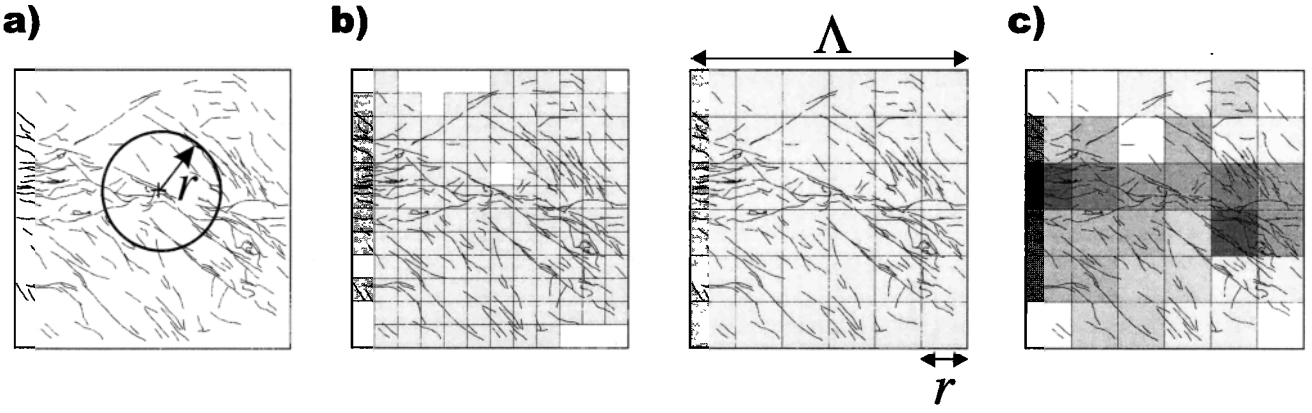

Figure 3. Classical methods used to calculate the fractal dimension. These are (a) the mass dimension, where the total length of fracture lying in a disk of radius r is calculated, and (b) the box-counting method, for which the system of size Λ is covered by a regular mesh of size r. Two different mesh sizes are shown, where boxes inside which fractures are present are shaded and empty boxes are open. In Figure 3c the multifractal analysis derived from the box-counting method for which each box of size r is weighted by the total length included in it. The darker the box, the greater the fracture length found inside it.

where the sum is carried out over all boxes and gives simply the total cumulative length of all fractures (Figure 3c). The moments of order q are then constructed:

$$M_q(r) = \sum_1^n [p_i(r)]^q \tag{13}$$

and should scale as $M_q(r) \approx r^{(q-1)Dq}$, where the set $\{D_q$ for $q = -\infty$ to $+\infty\}$ forms the "multifractal spectrum" of generalized fractal dimensions [*Hentschel and Proccacia*, 1983]. Note that $D_{q=0} = D$ by definition. The most widely used of these dimensions are called the *capacity dimension* ($q = 0$), the *information dimension* ($q = 1$), and the *correlation dimension* ($q = 2$). In general, multifractal measures give the distribution of physical or other quantities on a geometric support [*Feder*, 1988]. The multifractal spectrum can be determined for any measure, μ (not only the mass L), defined for the object. Note that the zero-order moment defines the object, not the measure. For more information on the use of multifractal methods the reader is referred to *Vignes-Adler et al.* [1991], *Davy et al.* [1992], and *Sornette et al.* [1993].

The previous methods can be applied either on the fractured domain, for which fractures are not individualized, or on the fracture set. For the fractal dimension of the fracture set, another useful method is the two-point correlation function, which describes the spatial correlation of the fractures. The two-point correlation function gives the probability that two points belong to the same structure. It is defined as

$$C_2(r) = \frac{1}{N^2} N_d(r), \tag{14}$$

where N is the total number of points and N_d is the number of pairs of points whose distance apart is less than r [*Hentschel and Procaccia*, 1983]. Thus this definition is based on a cumulative frequency. For a fractal population of points, $C_2(r)$ is expected to scale with r as r^{D_c}, where D_c is the correlation dimension of the system. This technique is easy to apply and has been used for fracture networks to describe the spatial distribution of fracture barycenters, which are defined as the midpoints of the fracture traces [*Davy et al.*, 1990; *Sornette et al.*, 1993; *Bour and Davy*, 1999]. Note that the box-counting method can also be applied to fracture barycenters. Theoretically, the correlation dimension in (14) is equivalent to the correlation dimension D_2, obtained with the box-counting method [*Hentschel and Procaccia*, 1983]. It is also possible to compute the correlation functions of triplets, quadruplets, ..., n-tuplets of points to obtain the higher-order dimensions D_3, D_4, and so forth.

A few studies [*Gillespie et al.*, 1993; *Walsh and Watterson*, 1993; *Brooks et al.*, 1996; *Ouillon et al.*, 1996; *Bour*, 1997; *Berkowitz and Hadad*, 1997] have tested the suitability of these different techniques for measuring the fractal dimension of a fracture pattern. Using the box-counting method, several authors showed that similar results could be obtained from natural fracture patterns and synthetic randomly distributed fracture networks [*Odling*, 1992; *Ouillon et al.*, 1996; *Hamburger et al.*, 1996; *Bour*, 1997; *Berkowitz and Hadad*, 1997]. *Odling* [1992] and *Berkowitz and Hadad* [1997] explained such results by the presence of a crossover region between dimensions of 1 and 2; these patterns are, in fact, nonfractal. Nevertheless, the derivation of an apparent dimension is also easily achieved due to several biases and pitfalls in the application of the method [*Walsh and Watterson*, 1993; *Ouillon et al.*, 1996; *Hamburger et al.*, 1996; *Bour*, 1997]. *Bour* [1997] showed that the two-point correlation function method was better at distinguishing natural from purely random patterns than the box-counting method. This illustrates some of the experimental diffi-

culties that may be encountered when applying simple methods, well tested on theoretical examples, to complex natural systems. As we shall see in section 5.2, such experimental difficulties are made worse when these techniques are applied to insufficient amounts of data.

4. PHYSICAL ARGUMENTS

The physics of fracturing has been studied over many years. One of the first inklings of *scale invariance* in faulting came from the observation of the Gutenberg-Richter law for earthquake magnitude m of the form $\log N = a' - bm$, where N is the number of earthquakes of magnitude $m + dm$, and a' and b are constants. Noting that magnitude is a logarithmic measure of seismic moment, and that typically moment scales as source volume, this represents a power law relationship similar to (5) [*Turcotte*, 1992]. For the typical case of seismometers acting as velocity transducers, this represents a power law scaling of fault source area $N(A) = A^{-b}$, where $N(A)$ is the number of sources with area A, and typically $b \approx 1$. When compared with (5), with $A = l^2$, we find $a \approx 2$. Thus earthquake sources are filling space in a way in which the number of sources at the scale l is inversely proportional to source area, similar to a set of tiles of different sizes [*Kanamori and Anderson*, 1975]. In laboratory tests based on acoustic emissions it is common to observe a tending to this limit, beginning with a higher value $a = 3$ at the onset of loading, reaching $a = 1$ at the moment of dynamic failure, and reaching steady state at $a = 2$. This and other aspects of scale-invariant behavior in the Earth and in laboratory tests were recently reviewed by *Main* [1996].

It is beyond the scope of the paper to review all the theories and different types of natural fractures that are encountered in the Earth; thorough discussion of these may be found in course books dealing with fracture in Earth systems [e.g., *Atkinson*, 1987; *Scholz*, 1990; *Lawn*, 1993]. Here we concentrate on the physical arguments that may underlie the geometrical distribution of fracture networks.

4.1. General Principles

Conditions for the formation of a rock fracture are related to critical thresholds of stress, or on stress-related energy or intensity, according to a number of different theories [*Griffith*, 1920; *Irwin*, 1960]. Whatever the fracture mode (i.e., the propagation mode), the stress distribution is a key factor in determining the geometry of the next stage of the fracturing process. Thus the stress distribution depends on the geometry of preexisting fractures and includes both stress enhancement at the fracture tips and stress release in the vicinity of the fracture planes. A typical case study is the propagation of an isolated crack in a homogeneous system, i.e., a system where the applied remote stress and the yield strength are spatially constant. Because of stress redistribution, a fracture creates the conditions for its own growth. The final stage is reached when the mechanical system is broken in two and the applied stress is totally released. This simple resulting geometry, however, is rarely encountered in the Earth for several reasons. First, the intrinsic heterogeneity of natural rocks allows several nuclei to propagate simultaneously, so that the resulting stress distribution becomes much more complex as a consequence of mutual crack interactions. Second, the applied stress field is not necessarily homogeneous. Indentation of a large continent by a smaller one is a typical example of heterogeneous boundary conditions. Third, fluid-rock interactions and/or internal residual stress may produce local variations in the stress field. All of these contribute to the complexity of natural fracture networks. The nature of the complexity, and of the resulting spatial distribution, however, is an open question. We explore some insights in the following paragraphs.

4.2. Arguments in Favor of Power Laws

The key argument in favor of power law distributions is the absence of a characteristic length scale in the fracture growth process. In the simplest model of an isolated crack in a homogeneous linear elastic system, the near-field stress distribution σ_{ij} is efficiently described by a function whose sole spatial parameters are r, the distance to the crack tip, and l, the crack length. The absence of other characteristic length scales leads *Sornette and Davy* [1991] to propose a simple formulation for the fracture length growth of the form $dl/dt \approx l^a$. In a system where a population of nuclei of different lengths exists, this simple growth model will produce a power law length distribution, with an exponent $-a$. They argue that $a = 2$ is relevant to natural fault distributions similar to that proposed for earthquake source lengths.

The assumptions of this simple model (isolated fractures and homogeneous mechanical properties) are too simplistic to account for realistic conditions. Further arguments are found in recent models that incorporate the role of disorder in the rupture process [*de Arcangelis et al.*, 1989; *de Arcangelis and Herrmann*, 1989; *Cox and Paterson*, 1990; *Charmet et al.*, 1990; *Herrmann and Roux*, 1990; *Hansen et al.*, 1991; *Lockner and Madden*, 1991; *Reuschlé*, 1992; *Vanneste and Sornette*, 1992; *Davy et al.*, 1995]. These models, based on concepts of statistical physics, have been developed by defining *universality* classes of rupture from scaling laws between the global properties of the networks of elastic (or electrical) elements and the size of the networks. The mode of rupture is defined by an interaction between stress enhancement effects at crack tips and the probability of finding a weaker or stronger bond in the medium. There exist only a few classes of behavior for which exponents, associated with each class, are independent of the details of the particular breakdown model that is used. *Hansen et al.* [1991] defined four types of behavior: (1) a regime with

one single crack (case of materials with no disorder), (2) a scaling regime with diffuse damage and localization, (3) a diffuse damage case, and (4) a regime of strong disorder. The conditions over which each type of behavior is dominant are governed by only two parameters, which characterize the distribution of the weakest and the strongest bonds. These models confirm the existence of power law distributions as an intrinsic characteristic of the breakage process arising from the initial heterogeneity of the material. Moreover, they predict a scale dependence of rock mass strength, a property that is commonly discussed by rock mechanists [*Heuze*, 1980]. However, because they are based on grid simulations, they consider the distribution of broken bonds rather than the fracture distribution.

Arguments on fracture distributions may be found in recent numerical models [*Cowie et al.*, 1995; *Poliakov and Hermann*, 1994; *Poliakov et al.*, 1994; *Nielsen et al.*, 1995; *Cladouhos and Marrett*, 1996] or lithosphere-analogue experiments [*Davy et al.*, 1995; *Bonnet*, 1997] that explicitly consider the fracture as a breaking entity. Many of these studies found the fracture density to be fractal, with a fractal dimension of about 1.7 in two-dimensional (2-D) systems and the fracture length distribution to be adequately modeled by a power law with an exponent of about -2. The lognormal distribution obtained by *Renshaw and Pollard* [1994] with numerical simulations may be interpreted as a snapshot of an intermediate stage of the fracture growth.

It is interesting to notice that these conclusions were obtained for different models of fracture growth. Some are static, and others incorporate a complete dynamical description of the physical phenomenon with seismic waves. Some are concerned with mode I (tensile) fracture; others are concerned with mode II (shear) faults. Another interesting result is that a complex fracture organization was also found in systems where the initial material heterogeneity is small (for instance, when the standard deviation of the yield strength is much smaller than the mean value). Examples can be found in the thermal fuse model of *Vanneste and Sornette* [1992], in the shear-band model of *Poliakov et al.* [1994], or in the experiments of *Davy et al.* [1995]. In all these studies, the breaking conditions are made widespread in the system due either to memory effects or to a short-range coupling between fractures.

A key question remaining concerns the relationships between fracture organization, fracturing mode, and the nature of the applied stress. Tectonic stresses are examples of stresses applied at the system boundaries. In contrast, internal stresses are responsible for joint formation in response to pressure decompression or thermal cracking. The deformation of concrete also appears as an industrially important problem of that kind. Most of the previous studies focus on tectonic stresses. To our knowledge, the sole study of the role of internal stresses is that of *Schmittbuhl and Roux* [1994], who showed that fractal scaling laws still apply, but with a change in the basic exponents. Pursuing this issue seems to be important for understanding the differences between faulting and jointing.

4.3. Length Scales in Fracture Patterns and Associated Physical Processes

The upper and lower bounds of any fracture size distribution are related to characteristic length scales either of the system or of some associated physical processes [*Mandelbrot*, 1982]. The question of a physical lower limit to fracture size has been rarely addressed, mainly because of the limitations of observation. Intrinsic limits may be due to atomic bonds or grain sizes, depending on the nature of the breaking materials. The distribution of material heterogeneities may be an interesting issue to explore with regard to this lower limit. *Henderson et al.* [1994] showed that a lower limit to power law scaling in the length distribution greater than the grain size could occur in fluid-saturated porous media. The upper limit has been more extensively studied, where the finite thickness of sedimentary beds and the brittle crust has been found to violate simple scaling-law behavior in fracture or earthquake distributions [*Pacheco et al.*, 1992; *Davy*, 1993; *Volant and Grasso*, 1994; *Ouillon et al.*, 1996].

Periodic or length-dependent organization has also been found in specific systems such as the bending of sedimentary beds [*Gross*, 1993; *Rives et al.*, 1992], the buckling of layers or *boudinage* instabilities [*Burg et al.*, 1992; *Martinod and Davy*, 1994], patterns in drying mud, hydrothermal cracks, cross joints [*Dyer*, 1988], and in some sandbox experiments [*Vendeville et al.*, 1987]. Here we review some of the reasons that these boundary conditions may lead to a length-dependent fracture organization.

The first reason may be found in systematic variations of the applied stress. A typical example is periodic instabilities that occur in thin layers suffering horizontal compression or extension in a gravity field [*Zuber et al.*, 1986; *Ricard and Froidevaux*, 1986; *Martinod and Davy*, 1992, 1994]. The lithosphere, for instance, can be considered as a laminated material with highly contrasting rheologies. Folding, buckling, and boudinage are expressions of these instabilities and preferentially develop near the inflexion points of folds [*Burg et al.*, 1992; *Martinod and Davy*, 1994]. The wavelength of the instability, which depends on the mechanical properties of the layers and a gravity term, is an intrinsic control on fault spacing.

Another example of systematic stress variations is found when a shear stress exists at the base of the fracturing layer. The balance of stresses predicts an increase of the stress components within the brittle layer which causes fractures to propagate with a dominant spatial period in order to maintain the stress below the yield strength of the brittle material. Examples can be found in sandbox experiments with a basal rubber sheet or with a basal flowing ductile layer [*Vendeville et al.*,

1987]. A sticking condition produces similar effects, as observed in experiments where a thin brittle coating is stretched over a bending elastic substrate [*Rives et al.*, 1992; *Wu and Pollard*, 1995].

The second major cause for finding a characteristic length scale is the existence of coupled physical processes. Brittle/ductile coupling, particularly relevant to lithosphere systems, was found to limit the power law distribution to a length scale related to the ductile viscosity [*Davy et al.*, 1995; *Bonnet*, 1997]. The propagation of seismic waves [*Poliakov et al.*, 1994] was also found to generate short-distance coupling that controls the average spacing between faults.

4.4. Power Laws in Natural Fracture Systems

Even if frequently observed, power laws are not the only possible distribution found in natural fracture systems. Observations of regular spacing in joints or faults are counterexamples for a total generalization of this kind of scaling property. However, power law distributions are physically sound in heterogeneous systems, and the frequent occurrence of this distribution may arise because of the intrinsic heterogeneity of Earth materials.

An important issue that has still not really been addressed is the relationship between scaling exponents, applied stress, and the mode of fracture propagation. The difference between "tectonic" stresses and internal stresses has already been invoked in the previous paragraphs. Another difference lies in the propagation mode of the fractures. Joints are considered to propagate in mode I, while faults correspond to mode II. Note that most faults grow in a direction parallel to the offset direction, except for crustal normal faults or thrusts, which propagate in a direction perpendicular to the displacement. These differences in the propagation mode induce significant differences in the network geometry in terms of orientation and fracture density. This may, but not necessarily, imply systematic differences in scaling exponents. In the absence of physically sound theories concerning scaling laws in natural fracture systems, a compilation of data is the only way forward to characterize and evaluate the significance of these laws.

5. SAMPLING ISSUES AND DETERMINATION OF THE POWER LAW EXPONENT

5.1. Sampling Effects

Because of the finite size of the sampled domain and the resolution of the technique used to map fracture systems, sampling effects at small and large scales may cause the frequency distribution of a power law population to deviate from the perfect straight line that would be observed for an infinitely large system. These are termed "truncation" and "censoring" effects, respectively.

5.1.1. Truncation effect. In the truncation effect, the frequency of small fractures is underestimated due to the resolution limitations of the sampling method used. Truncation effects are most easily identified in the density distribution $n(l)$ where the slope goes through zero and becomes positive for the smallest fractures rather than simply tending to zero as in the cumulative distribution $C(l)$. Most authors have simply removed the part of the distribution affected by truncation by, somewhat subjectively, fixing a threshold below which fracture traces are thought to be incompletely mapped [*Rouleau and Gale*, 1985; *Villaescusa and Brown*, 1992]. Analysis of truncation lengths for published distributions shows that these range from 5 to 25% of the map size (see section 6.3 for more details). However, at present, no quantitative methods exist for determining this observational threshold (see section 5.3).

Although resolution is thought to be the primary cause of deviation from a power law trend at small scales, other causes have also been suggested. *Heffer and Bevan* [1990] proposed that truncation effects could reflect an effect of a 2-D cut through a 3-D population and derived a function describing the total number of observable faults greater than a given length on a 2-D map surface. However, this function is based on the assumption that all properties of the fracture system are independent, which seems not to be the case, at least for position and length [*Ackermann and Schlische*, 1997]. Another possible cause for the deviation from a power law trend is the existence of a physical lower cutoff to the power law size population. *Odling* [1997] suggests a natural lower cutoff of around 1 m for the power law length distribution of joints in sandstones. Generally, however, there has been little attempt in the literature to evaluate naturally occurring upper and lower cutoffs to observed power law distributions.

5.1.2. Censoring effects. Deviations from power law frequency distribution trends for fractures with sizes comparable to the sampled region occur due to two separate sampling biases. The first is associated with the probability that long fractures that intersect the sample area boundary are incompletely observed, termed "censoring" effects. The second is related to the subjective choice of sample region which often tends to exclude the very largest fractures, for example, faults that bound an entire basin.

Several methods exist for correcting the mean of the population sample or deriving the parameters of the underlying distribution, but most assume a lognormal or exponential parent distribution [*Cruden*, 1977; *Priest and Hudson*, 1981; *Pahl*, 1981; *Einstein and Baecher*, 1983; *Kulatilake and Wu*, 1984] (see also *Laslett* [1982] for a review). The method of *Laslett* [1982] has been adapted for a power law by *Gil and Johansen* [1990], *Clark et al.* [1999], and *Bour and Davy* [1999]. Other methods such as the Kaplan-Meier filter have also been applied [*Lindsay and Rothrock*, 1995; *Odling*, 1997]; Kaplan-Meier has the advantage of being independent of the underlying distribution.

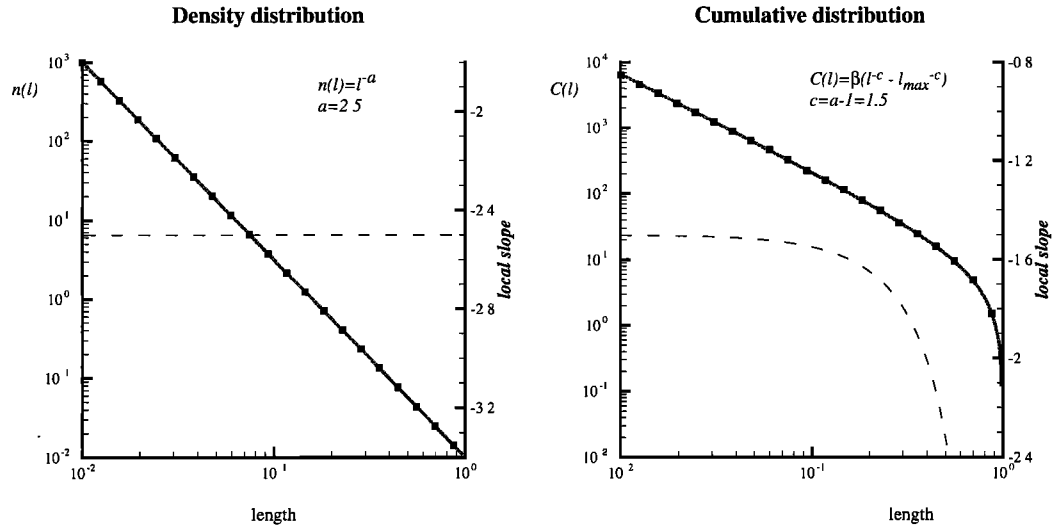

Figure 4. Illustration of the density $n(l)$ and cumulative distribution $C(l)$ for the same theoretical power law population with density exponent $a = 2.5$ and cumulative exponent $c = 1.5$. The slope of the trend is shown by the dashed curve. The curvature observed at larger fracture lengths in the cumulative distribution $C(l)$ is associated with the integral of the density $n(l)$. This curvature reduces the section of the cumulative distribution trend that shows a straight line (defining the power law) to over only 1 order of magnitude.

Pickering et al. [1997] have proposed another cause for the deviation from a power law trend at large scales based on the displacement of faults. Displacement varies along the fault length, generally decreasing toward the fault tip. The limit of detectable displacement results in an underestimation of all fault lengths and thus influences the estimated exponent. *Pickering et al.* [1997] proposed that fault lengths should be increased by a constant amount so that a linear relation between the length and its maximum displacement is obtained. However, although a linear relation between length and displacement is often observed [*Cowie and Scholz*, 1992a, 1992b; *Clark and Cox*, 1996], nonlinear relations have also been reported [*Fossen and Hesthammer*, 1997] (see section 6.4).

Sampling effects associated with the largest fractures can potentially lead to a shallowing of power law trends. If the location of the sample area is randomly chosen, the probability that it is intersected by a fracture of a given length increases with fracture length. Thus large fractures, only part of which may be present in the sample area, will be overrepresented. After correction for censoring effects, this lead to increased frequencies for long fractures and a shallowing of the power law frequency distribution trend. Such effects have been observed in natural data [*Ackermann and Schlische*, 1997] and have been analytically derived by *Bour and Davy* [1998]. They may also be the origin of the "characteristic earthquake" debate in seismology [*Main*, 1996].

The cumulative frequency distribution for power law fracture populations suffers from additional effects that lead to a curvature of the trend at large scales. By integrating the density distribution between maximum and minimum observed fracture lengths, we obtain for $C(l)$ the following expression:

$$C(l) = \frac{\alpha}{a-1}[l^{-a+1} - l_{\max}^{-a+1}]. \quad (15)$$

Here the upper bound $l_{\max}$ plays an important role. As l approaches $l_{\max}$, $C(l)$ approaches zero, causing a steepening of the trend. This behavior is intrinsic to $C(l)$ and is different from the censoring effects described above [*Pickering et al.*, 1995]. An example of this curvature and comparison with the density distribution are shown in Figure 4. This effect can significantly restrict the range over which the power law exponent can be estimated from cumulative frequency data. For a given exponent a, *Crave and Davy* [1997] have defined a critical length l_c, below which the deviation of $C(l)$ from a perfect straight line will be less than the error, ε. For example, if $a = 2.0$ and $\varepsilon = 10\%$, $l_c = l_{\max}/10$. Thus if the power law exponent is to be defined over 1 order of magnitude, no truncation effect must occur for fracture of length greater than $l_{\max}/100$ and data must be collected over more than 2 orders of magnitude. Failure to recognize such effects has often led to an overestimation of the exponent. *Pickering et al.* [1995] suggest a method to correct for this effect in which the number of largest faults is incremented until the falloff in the trend is reduced. The effect of curvature in a power law introduced by the size of the largest fault or joint spacing has also been discussed by *Ouillon et al.* [1996], and they proposed two theoretical methods to account for the downward curvature. This finite size effect can also lead to the spurious appearance of changes in scaling for large earthquakes [*Main*, 2000].

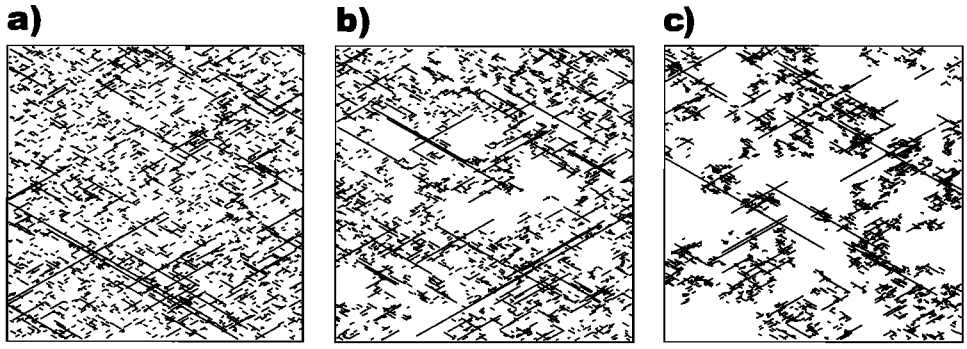

Figure 5. Fracture networks presenting the same length exponent (a = 2.7) and different fractal dimension D: (a) D = 2, (b) D = 1.75, and (c) D = 1.5. The number of fractures in each set is 2000. The method used for generating a synthetic fractal network is described by *Bour and Davy* [1999]. For these synthetic examples, only the spatial distribution of fracture barycenters is fractal, while the distribution of the fractured domain is not necessarily fractal.

5.2. Spatial Distributions and Topological Dimension

In recent years, the term "fractal" has been widely used in the literature to describe any kind of fracture feature following a power law distribution, such as length, displacement, and aperture distributions. A simple theoretical model of fragmentation (more generally known in physics as the Appolonian model) that gives rise to a power law length distribution was originally proposed by *King* [1983] and *Turcotte* [1986, 1992]. They then equated this exponent with the fractal dimension of the system. Following this, numerous authors have concluded that their networks are fractal if the length distribution is power law. In fact, the term fractal should be used only to describe the spatial distribution of fractures [*Mandelbrot*, 1982]. A fractal network implies a spatial correlation and organization between fractures that may be quantified through the fractal dimension and is independent of the distributions of other fracture features (Figure 5). Conversely, fractures may be randomly distributed in space (i.e., nonfractal) while other fracture features, such as lengths or displacements, can follow power law distributions (Figure 6) [*Bour and Davy*, 1997].

A few studies have analyzed both the spatial and length distributions of fracture networks [*Davy et al.*, 1990, 1992; *Sornette et al.*, 1993]. Recently, *Bour and Davy* [1999] have shown that the fractal dimension D and the *length exponent* a are related through the relation $D = (a - 1)/x$, where x is the exponent relating the average distance from a fracture barycenter to its nearest neighbor of larger length. The case of $a = D + 1$ in the fragmentation model of *King* [1983] and *Turcotte* [1986] corresponds to the particular case for which x = 1 and is a *self-similar* system. This relation, $D = (a - 1)/x$, has been verified by *Bour and Davy* [1999] for the San Andreas fault system and provides a useful method of testing the compatibility of fractal dimensions and the length exponent of a fracture pattern.

Statistical analysis techniques may be applied to 1-D, 2-D, and 3-D data sets. One-dimensional data are provided by well logs and scan lines, 2-D data are provided largely from outcrop maps and other images, and 3-D data are from seismic surveys and serial sectioning in, for example, quarries [*Gervais and Genter*, 1991; *Gertsch*, 1995]. At the present time, however, 3-D data sets seldom contain sufficient data to achieve a robust statistical

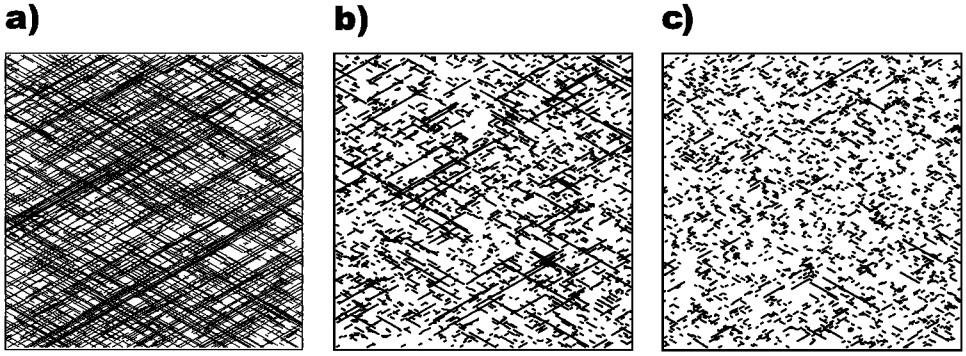

Figure 6. Fracture networks representing the same fractal dimension (D = 2) and power law length distributions with a different exponent, a: (a) a = 1.5, (b) a = 2.5, and (c) a = 3.5. The number of fractures in each set is 2000.

analysis. Spatial distributions have been studied on both 1-D and 2-D data sets, and length distributions have been studied largely through 2-D data sets. Other size distributions (i.e., aperture, width, or displacement) have been studied largely in 1-D. It remains one of the major challenges in the study of fracture systems to extrapolate results obtained from 1-D and 2-D data sets to 3-D systems.

Studies to date have concentrated on fracture length distributions. The relationship between the 3-D length (fracture diameter) distribution and the trace length distribution observed in a plane is already well established for the case of spatially randomly distributed discs where disc orientation and diameter distributions are independent [*Kendall and Moran*, 1963; *Warburton*, 1980; *Charlaix et al.*, 1984; *Clark et al.*, 1999]. When the size distribution of the disks follows a power law, trace lengths in an intersecting plane are also power law with an exponent, a_{2D}, equal to $a_{3D} - 1$ [*Marrett and Allmendinger*, 1991; *Westaway*, 1994; *Marrett*, 1996; *Piggott*, 1997; *Berkowitz and Adler*, 1998]. Similarly, the length distribution of ideal fractures intersecting a line will also follow a power law with an exponent a_{1D}, equal to $a_{3D} - 2$. The extrapolation to 3-D exponents for other fracture features such as aperture, width, and displacement has not been investigated for power law distributions and thus requires knowledge of the correlation of these features with fracture length [*Marret and Allmendinger*, 1991; *Westaway*, 1994; *Marrett*, 1996]. In a similar vein, the intersection of a 3-D fractal by a plane results in a fractal with D_{2D} equal to $D_{3D} - 1$, according to fractal theory [*Mandelbrot*, 1982]. Similar relationships are expected for scan lines with $D_{1D} = D_{3D} - 2$.

However, the above relations have been established for ideal Euclidean shapes or fractal sets, assuming that all the geometric parameters of the fracture system are independent and homogeneous. These assumptions may be not valid in many cases, because, for example, correlations between fracture position and fracture length have been demonstrated [*Ackermann and Schlische*, 1997; *Bour and Davy*, 1999]. From a theoretical analysis of reconstructing 3-D exponents from synthetic 1-D and 2-D data, *Borgos et al.* [2000] derived the equation

$$\xi_{3D} = \xi_{2D} + B, \tag{16}$$

where ξ is the exponent and $0 \leq B \leq 1$. *Hatton et al.* [1993] compared scaling exponents from acoustic emission data (3-D) and direct fracture trace data (2-D) in subcritical tensile crack growth experiments in the laboratory. They showed that a combination of preferential crack nucleation at the tensile surface and directional fracture anisotropy resulted in a scaling equation of the form

$$\xi_{3D} = A \times \xi_{2D} + B, \tag{17}$$

where the best fitting line to the whole data set gave $A = 1.28 \pm 0.30$ and $B = -0.23 \pm 0.36$ (error bounds are one standard deviation). Thus extrapolations from 1-D and 2-D to 3-D systems are not as simple as the above theoretical models suggest. This has strong implications for inferences from 2-D observations of joint and fault sets and is likely to be a more severe problem when estimates are based on 1-D borehole data. Extrapolation from 2-D to 3-D remains an interesting challenge for future work.

5.3. Estimation of Scaling Law Exponents

In practice, scaling law exponents and fractal dimensions are estimated by first assuming the statistical validity of the power law over a certain scale range and then fitting a straight line to this portion of the graph on a log-log plot. The accuracy of the estimated exponent or fractal dimension depends on the validity of the initial assumption, on the size of the initial population sample, on the number of points in the log-log graph, and on the errors of measurement associated with these points. In any statistical analysis the quantity of data is crucial for the determination of the distribution type and its parameters. There are two aspects to the number of data used. The first is that the sample should be large enough to give a statistically acceptable representation of the population. The second is that the number of points on the frequency graph should be enough to allow a good statistical fit to the theoretical distribution. In addition, for power law distributions it is generally accepted that a range of values over 2–3 orders of magnitude should be sampled for good definition of the exponent.

Priest and Hudson [1976] estimated that the minimum number of fracture trace lengths required to determine the parameters of an exponential distribution is 200. *Warburton* [1980] concluded that 209 traces were not enough to allow a complete stereological analytical treatment. *Berkowitz and Adler* [1998], using the same analysis technique, found that the lower limit was 100 traces for "simple" cases (constant fracture size) but that for more realistic cases, more fractures are needed. *Childs et al.* [1990] tested the robustness of their techniques to the number of data for multi-scan-line displacement measurements. They found that the line segment on which the power law was defined persisted down to samples of only 137 measurements.

An accurate estimation of the number of fractures required depends on the exponent a. The larger the value of a, the steeper the graph and the greater the number of fractures needed to define an exponent over a given scale range. However, the generally accepted rule that the exponents should be defined over 2–3 orders of magnitude is rarely met. Although fractures may be sampled over 2 orders of magnitude, problems caused by truncation and finite size effects mean that the exponent, in practice, is often determined over a scale range of only 1 order of magnitude. There are often severe practical problems in extending the scale range of sampled fractures sufficiently to meet the above requirement. In practice, therefore, we suggest the simple rule

that a minimum of 200 fractures be sampled to adequately define exponents of power law length distributions, as an initial guide.

One way of extending the scale range over which the exponents are determined is to map the same fracture system at different scales and resolutions. This has been done in a few cases [*Yielding et al.*, 1992; *Scholz et al.*, 1993; *Castaing et al.*, 1996; *Line et al.*, 1997; *Odling*, 1997] and has enabled determination of the length distribution exponents over scale ranges up to 4–5 orders of magnitude. In making such compilations, care must be taken to note any naturally occurring upper and lower bounds to scaling laws that may correspond to changes in fracture type (joints, faults), fracture age, or deformation mechanism. *Ouillon et al.* [1996] in an analysis of fractures of the Arabian Platform found that the fracture length scaling was influenced by layering on a variety of scales from bedding to brittle crustal thickness. *Odling* [1997] found a length distribution for joints over a scale range of 2 orders of magnitude with a natural lower cutoff occurring at around 1 m. An additional problem with compilations of data is the method in which they are combined. The above authors have simply normalized the distribution with respect to mapped area (R^2). However, *Davy et al.* [1990, 1992] show that the number of fractures in the interval [l, $l + dl$] is proportional to the size of the mapped region to the power D (R^D), where D is the fractal dimension. This has implications for the manner in which distributions in such compilations are combined that have not yet been considered.

Fractal dimensions have very often been deduced from graphs with very few data points [*Gonzato et al.*, 1998]. This is due partly to the extensive use of the box-counting technique, where box sizes are progressively subdivided by a factor of 2. This scheme generates only seven points over a scale range of 2 orders of magnitude. However, many more points may be generated if a subdivision scheme based on a regular sampling on a logarithmic scale with a different base is used [*Walsh and Watterson*, 1993]. In the case of fractal dimensions and power law distributions for fracture length, displacement, or aperture, quoted errors on exponents refer most often to the correlation coefficient or standard deviation for the fit of the graph to a straight line using the method of least squares [*Gonzato et al.*, 1998]. Almost all correlation coefficients reported in the literature are greater than 0.97, and standard deviations are less than 0.05. Such seemingly high levels of accuracy are often used to validate a power law or fractal model. However, the least squares method starts by assuming that a straight line is the appropriate model for the trend, and it can be easily shown that nonfractal data sets can lead to seemingly accurate results if only a few points, defining a smooth, gentle curve, are used [*Berkowitz and Hadad*, 1997]. This spurious statistical significance is exacerbated by the use of the cumulative distribution [*Main*, 2000]. In such cases, the value of the exponent obtained is meaningless and entirely dependent

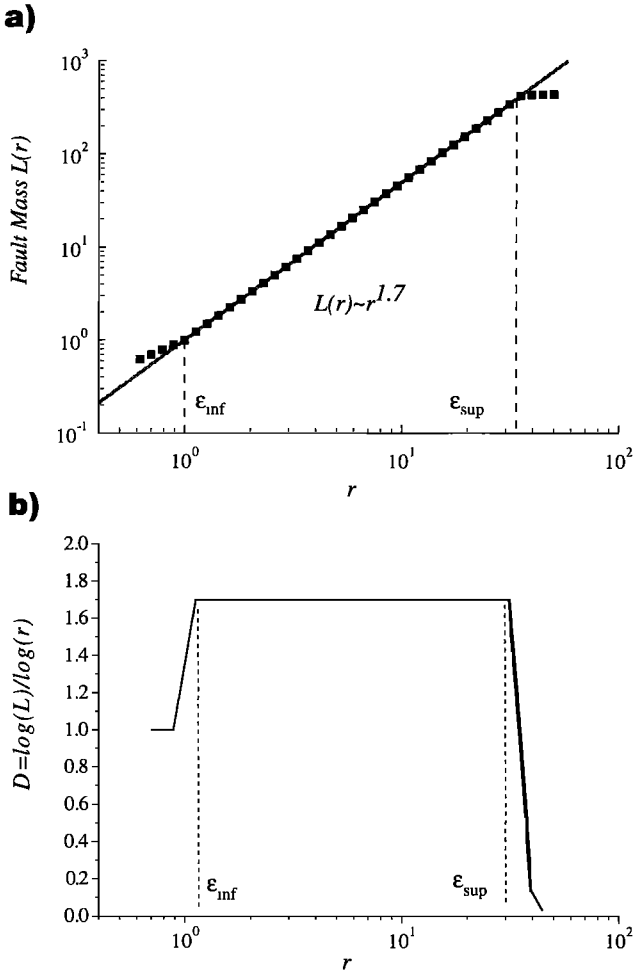

Figure 7. (a) Diagram illustrating a plot of fault mass in disks, $L(r)$, as a function of the disk radius r for a theoretical fractal fracture system, and (b) evolution of the local slope in Figure 7a as a function of r. The presence of the plateau indicates that the dimension is well defined between the upper and lower cutoffs, ε_{inf} and ε_{sup}.

on the scale range of points. Thus before applying the least squares method to determine the exponent, it is important to test whether a straight line is a good model for the trend.

A useful aid to evaluating the validity and value of power law exponents and fractal dimensions from log-log plots is to look at the local slope of the graph [*Chiles*, 1988; *Davy et al.*, 1990; *Odling*, 1992; *Walsh and Watterson*, 1993; *Gillespie et al.*, 1993]. A simple visual inspection of a plot of the local slope against the measured quantity reveals any plateaus which indicate scale ranges over which the slope of the graph can be considered constant (Figure 7). This method provides an indication of the scale range over which a fit to a straight line should be made by linear regression and provides a check on the validity of the estimated exponent. If the local slope does not show any significant plateau, power law behavior is not demonstrated and no meaningful exponent can be determined. The fluctuation of the local slope also provides an estimate of the uncertainties in

the estimated exponent. Although this method has been widely used in the physics literature, it has been little used in the analysis of fracture networks.

In addition to the problems of determining the best model for the trend, the errors estimated by the least squares method do not include errors in the data points themselves and thus give a false impression of the level of accuracy. Where averages are computed in the analyses (such as the average mass of fractures included in a disc of radius r), the standard deviation of each data point may be easily computed as a function of r. However, if simple counts are computed (such as the number of boxes required to cover the system or the number of fractures within a length bin), there is no direct way to estimate errors in data points. As a consequence, the effects of uncertainties in the data points themselves are often neglected.

Some tests of the sensitivity of the box-counting method have been conducted. *Odling* [1992] compared results from a natural pattern with those from synthetic fracture networks having the same length and orientation distribution but randomly distributed in space and found only minor differences, both sets of data showing a crossover between the dimensions of 1 (the dimension of a single fracture) and 2 (the topological dimension). A simple rule can be used to estimate the scale above which the dimension of the fracture pattern must be 2 when using the box-counting technique, which is to find the largest unoccupied box that can be placed on the fracture system. For box sizes greater than this, the dimension of the system is 2 (all boxes are occupied). *Ouillon et al.* [1996] used a method similar to that of *Odling* [1992] to correct their analysis for the effect of the sampled area shape. Failure to take into account the shape of the sampled domain (which can be complex in outcrop maps due to limited *exposure*) can have a strong influence on the results obtained using the box-counting method [*Walsh and Watterson*, 1993; *Ouillon et al.*, 1996]. Using the simple test of *Odling* [1992], *Bour* [1997] tested techniques for determining different fractal dimensions using a number of fractures patterns (joint and fault systems). He concluded that the two-point correlation function was the only method able to properly discriminate between a random and a fractal distribution (Figures 8 and 9).

The above and sections 3 and 5 can be used to construct some simple guidelines for estimating power law exponents and fractal dimensions. For power law exponents, samples of around 200 fractures or more should be collected. Here both the density and cumulative distributions should be plotted for comparison, and the method of *Davy* [1993] can be used to choose a suitable bin size for the density distribution. For fractal dimensions, ensure that the analysis generates a sufficient number of points on the graph. For power law exponents, identify a truncation cutoff using the density distribution and correct for censoring using the methods outlined by *Gil and Johansen* [1990], *Odling* [1997], *Clark et al.* [1999], or *Bour and Davy* [1999]. In addition, corrections for finite size effects using the method of *Pickering et al.* [1995] can be made. Plot the local slope of the graphs and use this to determine the scale range or ranges over which the trend can be considered to approximate a straight line. For power law exponents, plot the local slope of both the density and cumulative distributions, which should differ by 1. At this stage, a possible conclusion may be that a power law or fractal model is not appropriate for the data. If a scale range can be identified within which the slope can be considered constant, the points within this scale range can be then fitted to a straight line using statistical fitting techniques such as linear regression.

6. SYNTHESIS OF DATA ON FRACTURE LENGTH DISTRIBUTIONS

In this section we review the analyses of power law fracture length distributions from the literature. The data come from three main sources: physical experiments, numerical simulations, and observations of natural systems (outcrop, seismic, photograph and satellite image data). Exponents from observations of natural systems are the most numerous and we concentrate largely on this group, but physical and numerical experiments provide additional information on the evolution of fracture length distributions with time and are therefore discussed first.

6.1. Physical Experiments of Fracture System Development

Experiments have been conducted in four main types of material: sand (with or without a basal silicon putty layer), clay, plaster, and rock. These experiments allow the evolution of the fracture system evolution to be studied in relation to bulk strain, material type, rheological contrasts, and experiment size.

In sand or sand/silicon putty experiments, fractures are generated in a layer of loose sand, sometimes overlying a ductile material like silicon putty which applies close to a homogeneous strain to the undersurface of the sand layer. Here *Sornette et al.* [1993] found that the exponent of the fracture length distribution appears to depend on the degree of maturation of the network, i.e., on the applied strain. For fractures in the length range 10–100 mm, the exponent varied from 1.7 to 2.6 but approached a value of 2.0 at high strains. In similar experiments, *Davy et al.* [1995] and *Bonnet* [1997] have shown that the nature of the length distribution depends on the deformation regime. Where deformation is uniformly distributed, the length distribution is exponential, and where it is highly localized it is a power law with an exponent close to 2. Between these two cases, it is a gamma law (see section 2) with an exponent also close to 2.

In the experiments of *Walmann* [1998], a thin layer of

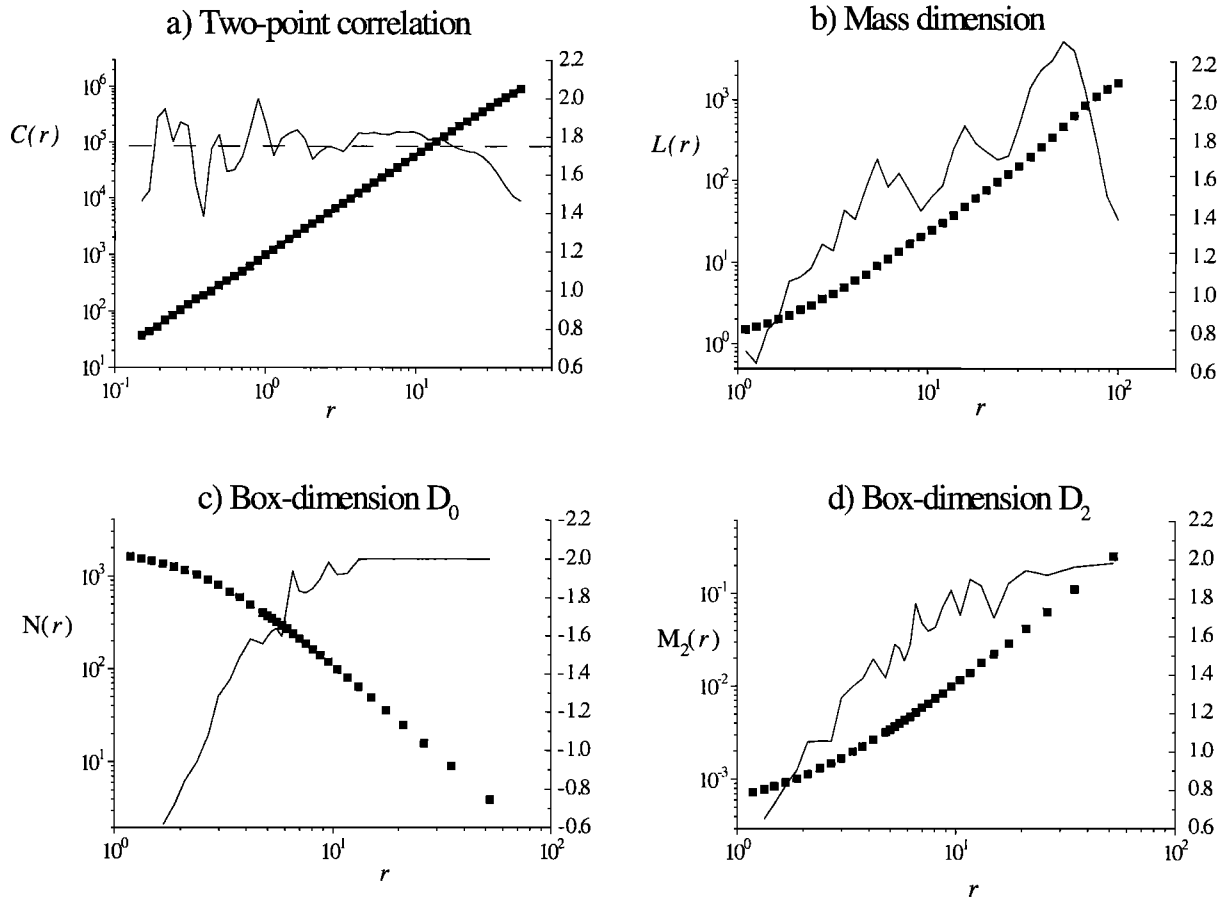

Figure 8. Example showing the determination of the fractal dimension for the fracture network presented in Figure 5b (2000 fractures, $a = 2.7$ and $D_2 = 1.75$) using different methods. Each fracture trace is defined by its barycenter. (a) The plot for the two-point correlation function has a well-defined plateau, and linear regression gives $D_2 = 1.76$. (b) The plot for the barycenter mass dimension D_M shows large variations in local slope with no plateau. (c) The plot for the barycenter box dimension D_0. The local slope shows a plateau for the last few points around 2. (d) The plot for the barycenter box dimension D_2, where the local slope shows no plateau. Where no plateau is visible, no fractal dimension can be determined.

clay was stretched to produce a system of tension fractures whose lengths, after correcting for censoring effects, were found to follow an exponential law. Walmann then suggested that a power law could result from the interaction of several exponential laws. On the basis of five experiments in clay to generate fault systems, *Reches* [1986] observed that with increasing deformation, there is a transition from a power law distribution to a lognormal law. He suggests that this transition reflects the fracture density where developing systems (low density) exhibit power laws and mature systems (high density) display lognormal laws. However, the appearance of a lognormal law may be related to external limitations imposed by the finite size of the experiment (45 mm), because in later stages, long fractures (about 40 mm) have reached the experiment boundaries and ceased to grow so that subsequent nucleation and development of small fractures leads to a lognormal length distribution.

In experiments in rock samples, *Krantz* [1983], *Lockner et al.* [1992], and *Moore and Lockner* [1995] analyzed the length distribution of microcracks. They found that the density of microcracks was greatest close to the main fracture and that small microcracks tend to cluster around longer ones [*Lockner et al.*, 1992]. Similar observations have been made on natural fault systems [*Anders and Wiltschko*, 1994]. In tensile double torsion fracture laboratory experiments, *Hatton et al.* [1993] found a power law length distribution for microcracks with an exponent that depended on the fluid content of the rocks. The exponents were 2–2.5 for dry experiments and 2–2.7 for wet experiments, with higher exponents being associated with more distributed damage.

6.2. Numerical Simulations

Numerical simulations of fracture system growth, like the physical experiments, suggest that length distributions may evolve during the deformation process. *Cowie et al.* [1993a] found that the length distribution follows an exponential law during the first increments of deformation which, when fractures begin to interact, evolves

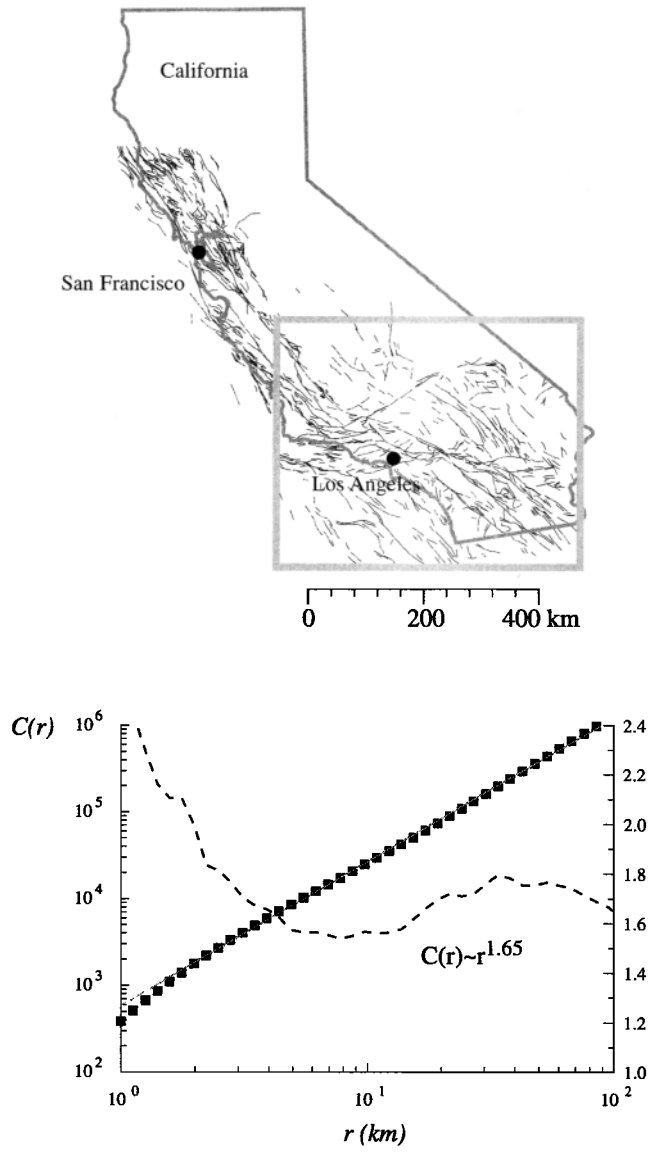

Figure 9. Example of a fault pattern from the San Andreas fault system with the corresponding two-point correlation function analysis. The slope of the graph (dashed curve) gives the fractal "correlation" dimension of the fault pattern and is defined over 1.5 orders of magnitude. The pattern contains nearly 4000 fault traces. Modified from *Bour and Davy* [1999].

toward a power law. The value of the exponent depends on the degree of deformation and tends to decrease with increasing strain [*Cowie et al.*, 1993a, 1995; *Cladouhos and Marrett*, 1996]. This indicates that with time the system contains progressively fewer small faults, implying that the processes of growth and connection dominate over nucleation. *Cowie et al.* [1995] found that at the final stage of rupture, the length exponent a lay in the range 2.0–2.4. A similar exponent of $a = 2.1$ over 1 decade was found by *Poliakov et al.* [1994] in a model based on plastic shear band growth. However, *Cladouhos and Marrett* [1996] have suggested that it is the system size that limits the exponent and that for very large systems exponents should be continually evolving.

6.3. Natural Data

Information on the distribution of fracture sizes comes from 1-D, 2-D, and 3-D data sets. One-dimensional data sets consist of the trace lengths of fractures that intersect a scan line [*Cruden*, 1977; *Priest and Hudson*, 1981] and can be sensitive to the orientation of the scan line [*LaPointe and Hudson*, 1985]. For all these 1-D data sets, the reported distributions are exponential. The determination of fracture size distributions in 3-D requires very large data sets, which, despite progress in seismic and ground-penetrating radar imagery, are still rare in literature. In some cases the three-dimensional geometry of a fracture system has been constructed from maps of fracture traces at different levels for rock samples [*Gertsch*, 1995] or in quarries [*Gervais and Genter*, 1991]. However, the number of fractures remains too small to allow meaningful statistical analyses.

The vast bulk of information on fracture length distributions in the literature comes from 2-D maps composed of fracture traces in a plane intersecting a three-dimensional fracture system. These sections may be in any orientation but are most commonly horizontal or vertical. Maps have been created from field data, photograph or satellite image analysis, and seismic data and cover a wide range of geological settings. Many of these studies claim that the trace length distribution is power law, although others claim lognormal and exponential laws. *Odling et al.* [1999] found that where layering plays an important role in restricting joint growth, a lognormal distribution reflects the true length population of joints whereas in more massive rocks, a power law distribution was more appropriate.

Here we present a compilation of these distributions and their exponents. We have limited the exponents to those where the graph from which the exponent has been determined is presented, allowing an assessment of the validity of the estimated exponent (45 distributions). This sample includes exponents estimated from single data sets and a few compilations where data at a variety of scales from a single locality have been used [*Yielding et al.*, 1992; *Scholz et al.*, 1993; *Castaing et al.*, 1996; *Line et al.*, 1997; *Odling*, 1997]. The source articles and the parameters of the power law fracture length distributions are listed in Tables 2 and 3.

As discussed in section 5.1.1, there exist no truly objective methods for determining the lower limit to the scale range over which the length distribution exponent should be determined (truncation length). We have estimated truncation lengths from the presented graphs in the literature and plot them against sample area S in Figure 10. This figure shows that truncation length shows an overall linear relationship with the size of the mapped area ($S^{0.5}$, where S is the surface) over some 12 orders of magnitude and lies between 0.5% and 25% of the map size, with an average around 5%.

TABLE 2. Compilation of Power Law Exponents for Fracture Length Distributions

Reference	N_{faults}	*Length Range, m*	*Distribution Used*	*Exponent*	*Area, m²*	l_{min}, *m*	l_{max}, *m*	ℓ_c, *m*	*Type*
Bahat [1987]	107	0.7–2.5	number (linear bin)	$a = 1.74$	24	0.1	28.5	0.60	J
Bahat [1987]	121	0.6–2.3		$a = 2.11$	25	0.1	22.5	0.30	J
Bour and Davy [1999]	3499	4×10^3 to 70×10^3	density	$a = 1.88$	2.7×10^{11}	10^3	90×10^3	10×10^3	F
Gudmundsson [1987a]	120	600–5750	number (linear bin)	$a = 0.90$	8.25×10^7	40	5750	8×10^3	V
Gudmundsson [1987b]	101	1000–7700	number (linear bin)	$a = 1$	2.62×10^7	57	7700	8×10^3	V
Hatton et al. [1993]	~300	10×10^3 to 200×10^3	number (linear bin)	$a = 1.76$	···	7×10^3	180×10^3	10×10^3	F
Ouillon et al. [1996]	~380	3–30	density	$a = 1.90$	3433	3	30	1.0	J
Ouillon et al. [1996]	~350	700–7000	density	$a = 2.10$	1.26×10^8	220	10×10^3	650	J
Ouillon et al. [1996]	~1000	2.2×10^3 to 15×10^3	density	$a = 3.20$	1.6×10^9	380	15×10^3	11×10^3	F
Ouillon et al. [1996]	~1000	3.5×10^3 to 11×10^3	density	$a = 2.10$	1.65×10^{10}	2×10^3	30×10^3	11×10^3	F
Reches [1986]	~800	0.14–2.63	number (linear bin)	$a = 2.2$	25	6×10^{-2}	2.63	100	F
Scholz and Cowie [1990]	~380	20×10^3 to 100×10^3	number (linear bin)	$a = 2.10$	···	2.5×10^3	310×10^3	10×10^3	F
Scholz [1997]	~1700	3×10^3 to 30×10^3	number (linear bin)	$a = 2.02$	10^{10}	10^3	50×10^3	···	F
Segall and Pollard [1983]	~260	3–16	number (linear bin)	$a = 1.30$	8750	1	33	$l_C \gg l$	J
Segall and Pollard [1983]	~100	15–50	number (linear bin)	$a = 1.80$	2100	1	67	$l_C \gg l$	J
Ackermann and Schlische [1997]	873	4×10^{-2} to 15×10^{-2}	cumulative	$c = 1.64$	34	5×10^{-3}	20	0.2	F
Belfield [1992]	320	600–10,000	cumulative	$c = 1.61$	2.07×10^7	40	12×10^3	···	F
Cladouhos and Marrett [1996]									
Krantz [1988]	~50	150–1500	cumulative	$c = 0.67$	29×10^6	70	4×10^3	···	F
Kakimi [1980]	~180	1000–7000	cumulative	$c = 0.97$	280×10^6	300	12×10^3	···	F
Scott and Castellanos [1984]	~400	300–2000	cumulative	$c = 1.21$	120×10^6	40	9×10^3	···	F
Blackstone [1988]	~250	10×10^3 to 60×10^3	cumulative	$c = 1.11$	250×10^9	4500	22×10^5	10×10^3	F
Stewart [1980]	~400	15×10^3 to 50×10^3	cumulative	$c = 1.84$	290×10^9	5500	12×10^5	10×10^3	F
Cladouhos and Marrett [1996]	~70	7×10^3 to 25×10^3	cumulative	$c = 1.67$	3600×10^6	~1600	35×10^3	10×10^3	F
Cladouhos and Marrett [1996]	~150	7×10^3 to 25×10^3	cumulative	$c = 1.66$	5100×10^6	~1250	35×10^3	10×10^3	F
Cladouhos and Marrett [1996]	~200	7×10^3 to 20×10^3	cumulative	$c = 2.07$	6200×10^6	1000	35×10^3	10×10^3	F
Clark et al. [1999]	1034	360–4500	cumulative	$c = 1.51$	87×10^6	10	2×10^4	3	F
Fossen and Hesthammer [1997]	40	1–20	cumulative	$c = 0.60$	2×10^4	6×10^{-2}	100	6–10	SB
Gauthier and Lake [1993]	318	150–800	cumulative	$c = 1.42$	169×10^6	70	2×10^3	100	F
Gauthier and Lake [1993]	291	150–800	cumulative	$c = 1.69$	169×10^6	70	2×10^3	100	F
Gauthier and Lake [1993]	78	100–700	cumulative	$c = 1.10$	169×10^6	100	2×10^3	100	F
Knott et al. [1996]	218	0.31–0.93	cumulative	$c = 1.02$	1	0.02	6	300	F
Needham et al. [1996]	111	100–5500	cumulative	$c = 2.04$	8.4×10^7	200	6500	···	F
Odling et al. [1999]	~470	2–20	cumulative	$c = 0.80$	11.7×10^3	0.06	300	1.2	V
Pickering et al. [1997]	417	200–1000	cumulative	$c = 1.18$	60×10^6	40	4×10^3	300	F
Schlische et al. [1996]	201	3×10^{-3} to 10^{-2}	cumulative	$c = 1.40$	0.30	0.15×10^{-3}	5×10^{-2}	0.2	F
Villemin and Sunwoo [1987]	~100	4×10^3 to 30×10^3	cumulative	$c = 1.40$	6×10^8	7×10^2	3×10^4	1.5×10^3	F
Watterson et al. [1996]	1034	200–5000	cumulative	$c = 1.36$	87×10^6	10	2×10^4	3	F
Yielding et al. [1996]	~450	500–6000	cumulative	$c = 1.18$	220×10^6	70	20×10^3	5×10^3	F
Yielding et al. [1996]	~350	4×10^3 to 50×10^3		$c = 1.75$	1.5×10^9	~180	50×10^3	5×10^3	F
Yielding et al. [1996]	300	1500 to 20×10^3	cumulative	$c = 1.37$	···	100	25×10^3	10×10^3	F

Values of a cited in publications, where a is the density or frequency exponent and c is the cumulative exponent ($a = c + 1$). Where available, or if it could be deduced, we also report complementary information. Listed are the number of fractures in the sample, the length range over which the exponent has been measured, the exponent (a or c), the area, the density of fractures, the minimum and maximum length encounter in the pattern (l_{min} and l_{max}), the characteristic length (l_c), if present, and the type of fracture (F, fault; J, joint; V, vein; SB, shear band).

TABLE 3. Compilation of Power Law Exponents for Combined Fracture Length Distributions

Reference	N_{faults}	*Range, m*	*Distribution Used*	*Exponent*
Castaing et al. [1996]	...	20 to 10×10^3	cumulative/R^2	$\gamma = 2.34$
Line et al. [1997]	...	$30–10^5$	cumulative/R^2	$\gamma = 1.66$
Odling [1997]	...	10–100	cumulative/R^2	$\gamma = 2.10$
Scholz et al. [1993]	...	30–2000	cumulative/R^2	$\gamma = 1.3$
Yielding et al. [1992]	...	3×10^3 to 30×10^3	cumulative/R^2	$\gamma = 2.00$

List of references using combined length distributions to determine the overall length exponent, hereinafter called γ. All references use cumulative distributions.

The published exponents are plotted in Figure 11a, which shows the range of fracture trace lengths over which they were determined. Cumulative distribution exponents have been converted to density distribution exponents a for the purposes of uniform comparison (in fact, we recommend that this is always done to avoid ambiguity). These data sets cover a wide range of scales from centimeters to hundreds of kilometers. Most values, however, lie in the range 10^2–10^5 m, which corresponds to the typical scale of seismic surveys. The majority of exponents are from fault systems with relatively few from joint and vein systems. Exponents from fault systems are spread throughout the total scale range, whereas joint systems have been studied largely at outcrop scale. Exponents show a large scatter between 0.8 and 3.5, and there is no clear dependence on the scale of observation. A histogram of these exponents shown in Figure 11b shows that 70% of the exponents lie in the range 1.7–2.75, with a maximum around 2.0. No significant trends can be distinguished for the different fracture types (veins, joints, and faults).

It has been shown in section 5.3 that there are many pitfalls in estimating the exponent of the best fit power law to observed fracture length distributions. One of the main factors is the number of fractures (section 5.3), and there we suggest that a minimum of 200 fractures be sampled. This is a rather simplistic rule since the number of fractures required to define the exponent over a given scale range depends on the exponent (see section 5.3). However, it is applied as a simple way of reducing the number of published exponents to those that can be considered statistically most sound. Applying this criterion to the data presented in Figure 11a reduces the number of acceptable exponents to 32, which are plotted in Figure 12. This results in a similar scatter with most of

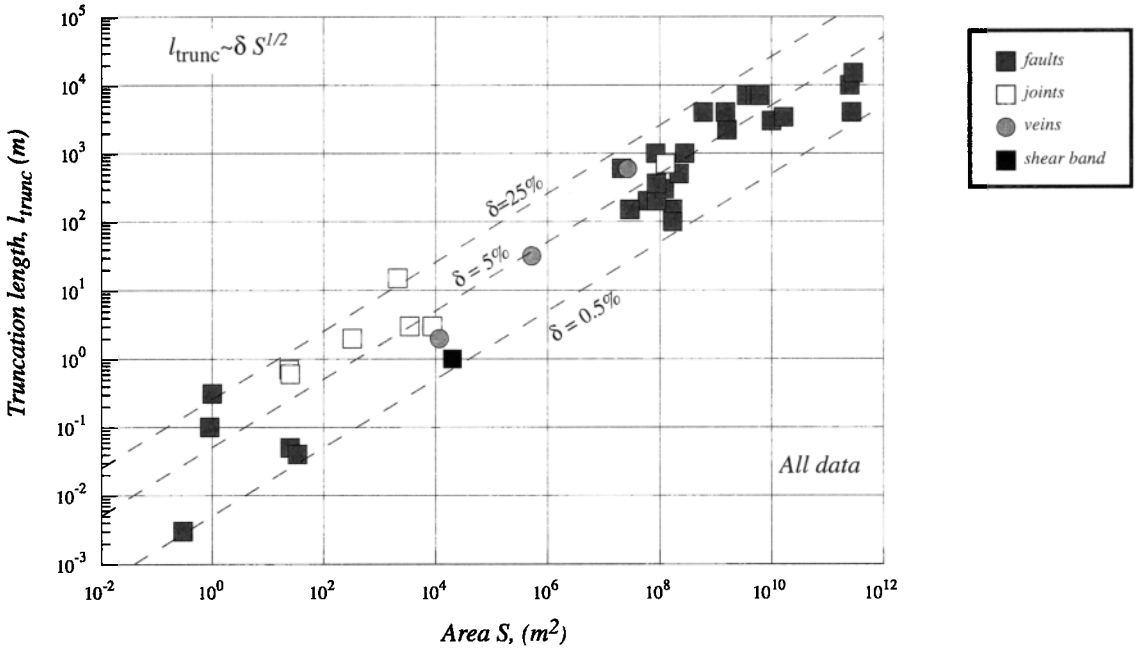

Figure 10. Truncation length l_{trunc}, corresponding to the lower limit of the length range over which the power law is defined, plotted against map area S. A linear trend can be defined over 12 orders of magnitude. Dashed lines give the upper and lower limits which lie at 25% and 0.5% of the map size. The average lies around 5%.

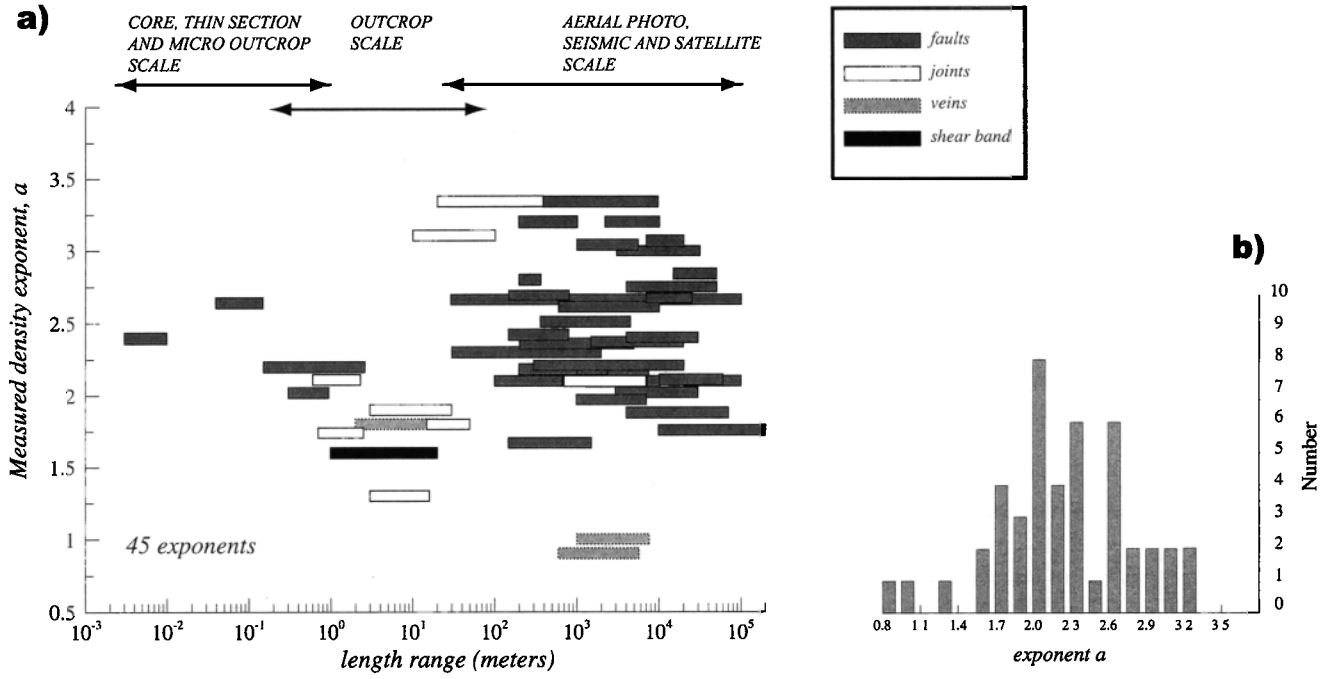

Figure 11. Synthesis of power law length distribution exponents from the literature. (a) Each density exponent is shown with respect to the length range over which it has been determined. The bulk of fracture data sets lie in the scale range for seismic, aerial photographs, and satellite images. Figure 11b is a histogram of exponent values. The exponents show a wide range from 0.8 to 3.5, with a maximum around 2.0–2.1.

the exponent values in the range 1.7–2.75, as in Figure 11, but with a greater concentration of exponents around 2.0. The relationships between the power law exponent a and other properties of fracture systems are further explored in the following sections.

The power law length distribution is defined by the exponent a and a constant, α. The constant α reflects the density of the fracture system:

$$N_F = \int_{l_{\min}}^{l_{\max}} n(l, R)\, dl = \int_{l_{\min}}^{l_{\max}} \alpha l^{-a} R^2\, dl, \qquad (18)$$

where N_F is the number of fractures per unit area and R is the size of the system. Computing the integral, and neglecting the term associated with the upper bound of the integral, gives for $a > 1$

$$N_F = \frac{\alpha}{a-1}\,(l_{\min}^{1-a} R^2), \qquad (19)$$

where $l_{\min}$ corresponds, in practice, to the truncation length l_{trunc}. From (19), α can be estimated by

$$\alpha = \frac{N_F(a-1)}{R^2 l_{\text{trunc}}^{1-a}}. \qquad (20)$$

In Figure 13a the constant α, computed for the published length distributions using (20), is plotted against map area S $(= R^2)$, and in Figure 13b it is plotted against the scale range over which the power law parameters were determined. These plots show no significant trend indicating that α is independent of the scale and resolution of the observations. Figure 13 shows an apparent slight decrease in α with scale, but the plot is heavily dominated by data sets at regional scales and it is thus uncertain if the trend should be considered significant.

Like the exponent a, α shows a wide range for all types of fractures (joints, faults, veins). In Figure 13c we look at the relationship between α, representing fracture density, and the length exponent a, which shows a positive correlation. Two trends can be interpreted in Figure 13c, suggesting that joint systems tend to show higher densities for a given exponent than fault systems. This agrees with the general observation that joint systems tend to be more distributed in space (space filling) than fault systems, which tend to be fractal (less than space filling), and gives a first clue to a means of quantifying systematic differences between different mechanisms of fracture propagation.

6.4. Relation Between Length and Other Fracture Parameters

6.4.1. Displacement distributions and length-displacement relationships. The distribution of displacement (throw) on faults and the relationship between displacement and length has been widely studied in the literature. Displacement distributions can be estimated through 1-D and 2-D sampling methods that give rise to

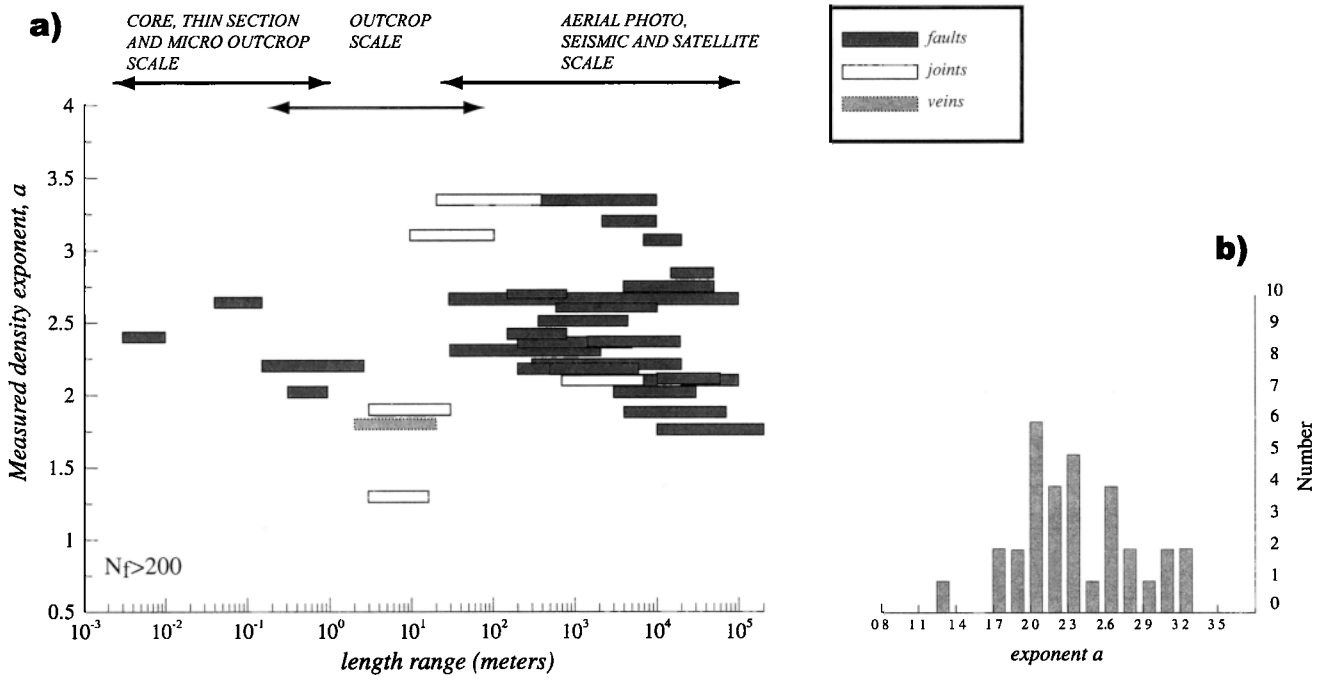

Figure 12. Length density exponents from the literature for samples with more than 200 fractures. (a) Each density exponent is plotted with respect to the range over which it has been determined. Figure 12b is a histogram of length exponent values. The total range of exponents has narrowed to 1.3–3.5 and shows a more distinct maximum at around 2.0–2.1.

different types of distribution. The distributions reported in the literature are frequently power law [*Childs et al.*, 1990; *Jackson and Sanderson*, 1992; *Pickering et al.*, 1996; *Steen and Andresen*, 1999] although exponential distributions also occur [*Dauteuil and Brun*, 1996].

In 1-D sampling, the displacement of a fault where it crosses a scan line is recorded (Figure 14a). Since the displacement varies along the length of a fault, the recorded displacement depends on where the scan line meets the fault and is not necessarily the maximum displacement for that fault. This method also tends to preferentially sample large faults, since these have the greatest probability of intersecting the scan line. Power law distribution exponents from 1-D sampling in the literature determined on cumulative distributions appear to lie in the range of 0.4–1.0 [*Gillespie et al.*, 1993; *Nicol et al.*, 1996; *Steen and Andresen*, 1999], i.e., 1.4–2.0 for the density exponent a. However, the relationship between these exponents and those where the maximum displacement has been recorded (2-D sampling) is not straightforward. A simple relation where the 2-D exponent equals the 1-D exponent plus 1 (see section 5.2) assumes that displacement and position are independent, which may not be the case [*Cowie and Scholz*, 1992a, 1992b; *Bour and Davy*, 1999]. Similar problems exist for multiline sampling where several parallel scan lines are used. This increases the number of data but means that long faults may be sampled several times (Figure 14b), which may explain the wider scatter observed for this exponent, which ranges from 1.3 to 2.3 (density exponent) [*Nicol et al.*, 1996; *Watterson et al.*, 1996].

In 2-D sampling, the maximum displacement found along each fault trace is recorded (Figure 14c). For this each fault must be identified, often a somewhat subjective process, and because sampling is most often done in 2-D sections through 3-D systems, this displacement may not represent the maximum for the entire fault plane. However, this method gives a more representative measurement than one-dimensional sampling, as a single representative displacement is attributed to each fault. There are only a few studies [*Villemin and Sunwoo*, 1987; *Childs et al.*, 1990; *Scholz and Cowie*, 1990; *Gauthier and Lake*, 1993; *Carter and Winter*, 1995; *Watterson et al.*, 1996; *Pickering et al.*, 1997; *Fossen and Hesthammer*, 1997] where the distributions are shown and can be evaluated for accuracy. These show a range of exponents from 1.7 to 2.4 with an average of 2.2 (Figure 15). A recent compilation *Yielding et al.* [1996] gave a similar average exponent of around 2.3.

The distribution of the maximum displacement from 2-D sampling allows comparisons to be made with length distributions. Fault lengths and displacements are generally positively correlated. The degree of correlation depends on many factors including fault interactions, but if for the sake of simplicity we assume a perfect positive correlation between length and displacement, the maximum displacement d_{max} will obey a power law of the form

$$n(d_{max}) = \beta d^{-t}, \tag{21}$$

and if d_{max} is related to the fault length l by

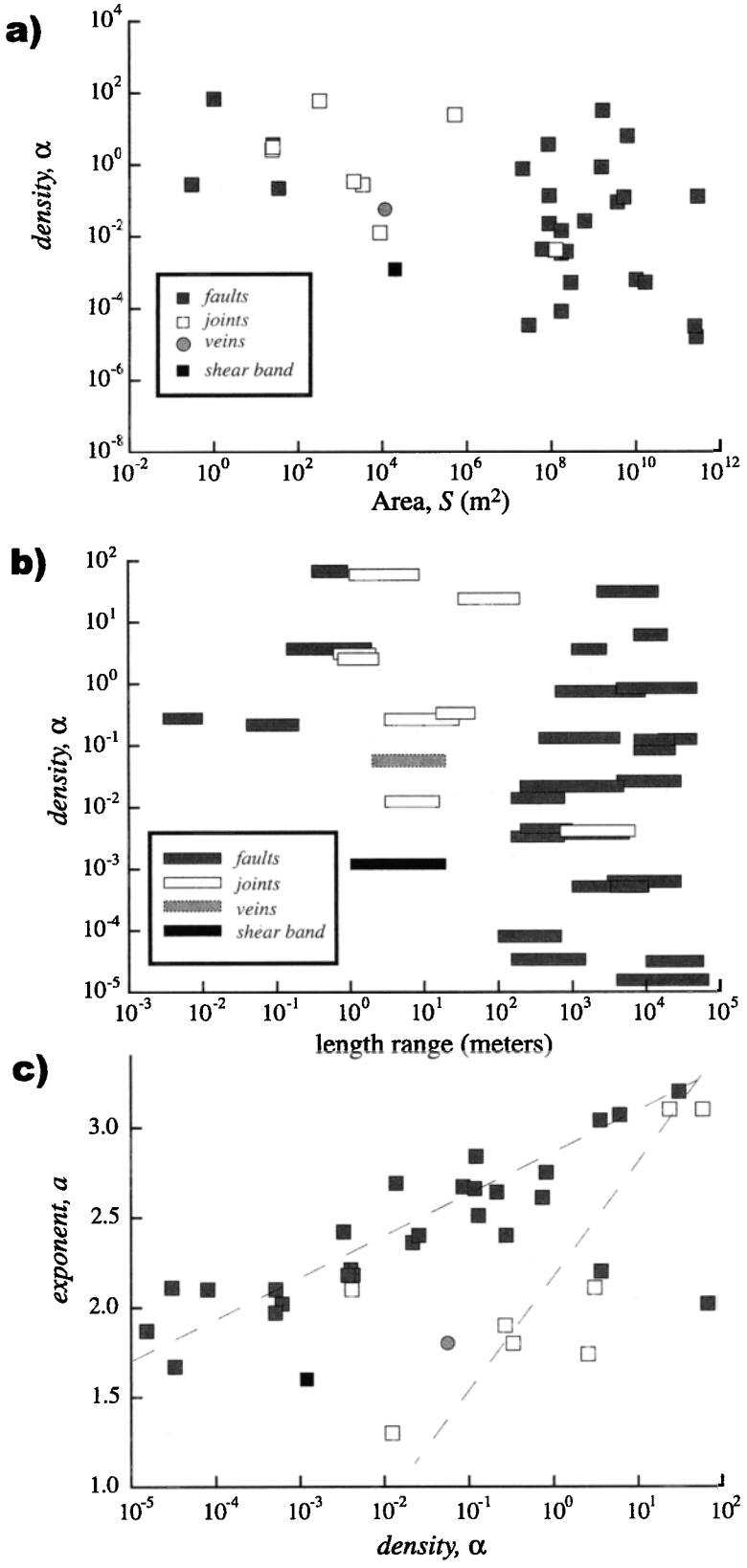

Figure 13. (a) Plot of the power law density constant α against the mapped area S. The plot is dominated by samples at regional scale, so it is uncertain if the apparent trend of a slight decrease in α with scale is significant. (b) Plot of the length range over which each length exponent is defined against density constant α. Values cover a wide range with no distinct difference between joint and fault systems. (c) Plot of density constant α against length exponent a. The plot shows two trends corresponding to fault systems, and joint and vein networks. This implies that for a given exponent, joint and vein systems tend to be denser than fault systems.

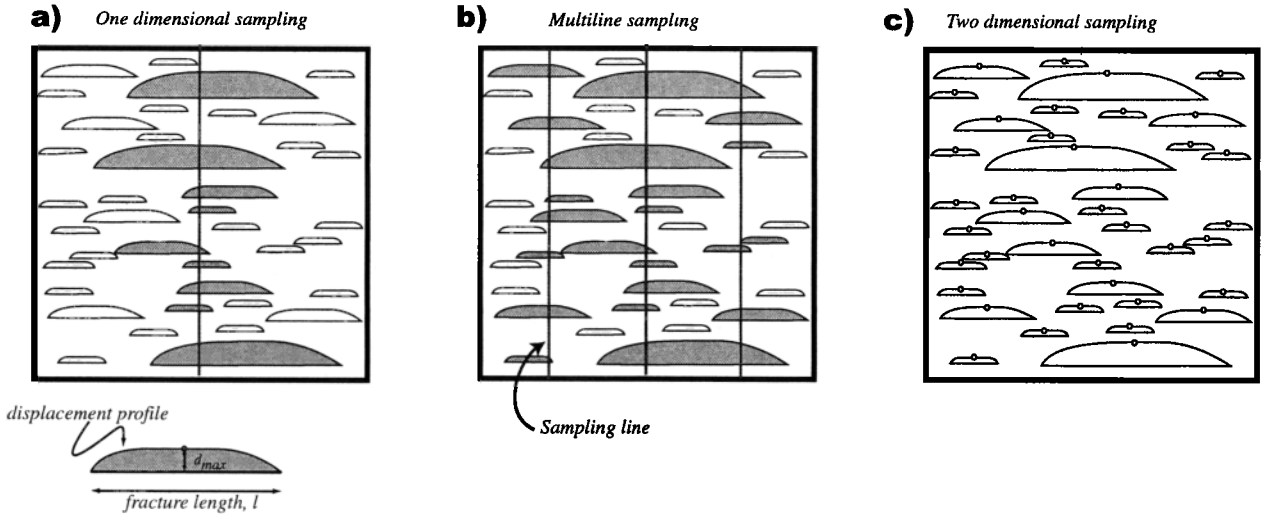

Figure 14. Illustration of one-dimensional sampling methods for fault displacement. (a) In one-line sampling, only displacements for faults which intersect the line are recorded (shaded fractures). These displacements do not necessarily correspond to maximum displacements for the faults. (b) In multiline sampling, the longer fractures can be recorded several times. (c) In 2-D sampling, the maximum displacement for each fault is recorded.

$$d_{\max} = \gamma l^{n_1}, \tag{22}$$

where β and γ are constant and t and n_1 are exponents, then the length and displacement distribution exponents, a and t, will be related by

$$a = n_1 t. \tag{23}$$

Simple elastic theory predicts a value of 1.0 for the exponent n_1 of the length displacement relation (equation (22)). However, a range of values for n_1 between 0.5

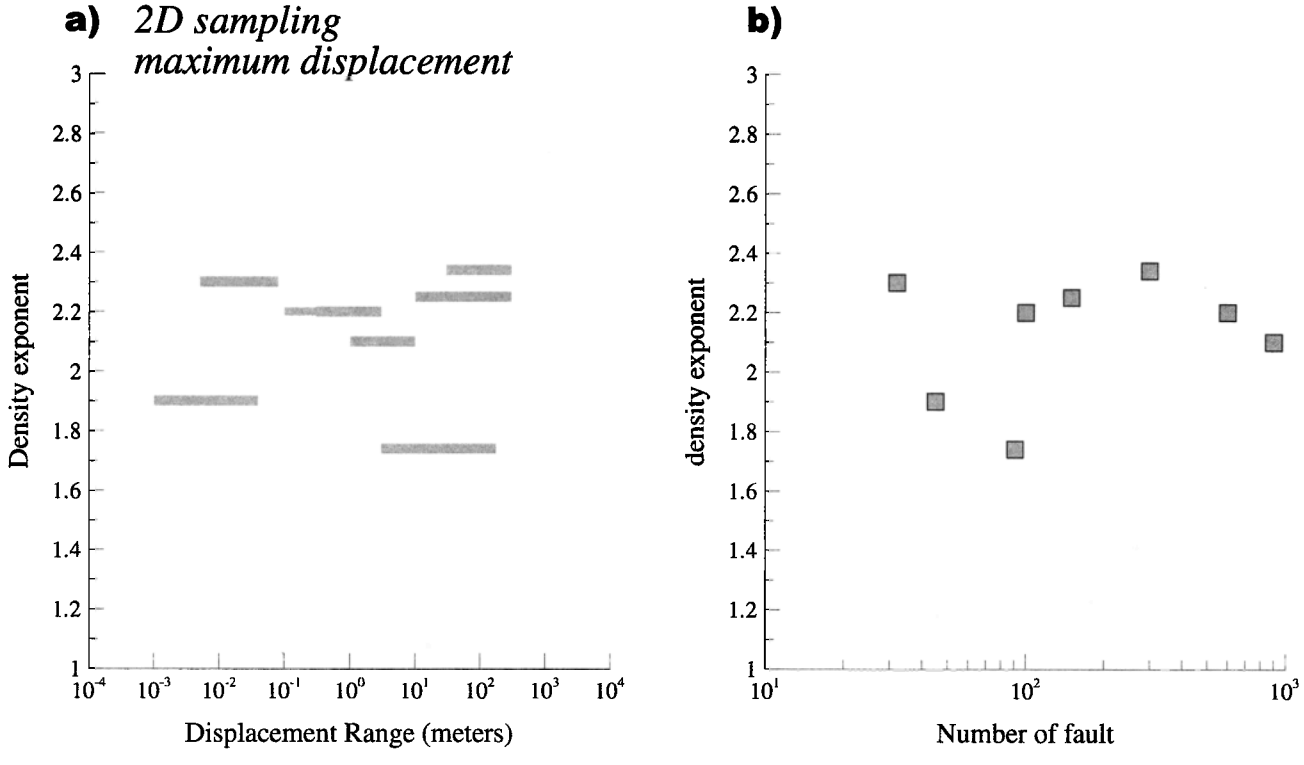

Figure 15. Synthesis of the maximum displacement distribution exponents with respect to (a) the range over which it has been determined and (b) the number of faults in the sample. The exponents show a range from 1.7 to 2.4 and show no significant correlation with number of faults in the sample.

and 2 have been proposed in the literature [*Walsh and Watterson*, 1988; *Cowie and Scholz*, 1992a, 1992b; *Gillespie et al.*, 1992; *Fossen and Hesthammer*, 1997]. Deviations from 1.0 can be due, in part, to scatter in the data and sampling problems but can also be attributed to physical causes, particularly interaction between faults. Linkage of fault segments can result in exponents of less than 1 [*Peacock and Sanderson*, 1991; *Trugdill and Cartwright*, 1994; *Cartwright et al.*, 1995]. Local heterogeneities, such as variations in the lithology, and finite size effects, such as the bed thickness [*Gross et al.*, 1997], and the fault growth mechanism may influence the nature of the length-displacement relation.

6.4.2. Aperture distribution and length-aperture relationship. Fracture apertures cover a wide scale range since the variation in apertures can result not only from mechanical misfit of fracture walls but also from chemical action such as dissolution, and normal pressure due to depth of overburden. Fracture apertures are also measured by a wide variety of methods, including direct measurements in core or outcrop and deduction from flow data, and therefore show a wide scatter. In the literature, aperture distributions are described as lognormal [*Snow*, 1970; *Hakami*, 1995; *Pyrak-Nolte et al.*, 1997] and power law [*Barton and Zoback*, 1992; *Belfield and Sovitch*, 1995; *Johnston and McCaffrey*, 1996; *Marrett*, 1996; *Sanderson et al.*, 1994]. In the power law case the aperture distribution can be expressed as

$$n(A) \approx A^{-z}. \tag{24}$$

Compared with studies of fracture length, there are relatively few studies of aperture distribution. For apertures in the range of millimeters to centimeters, *Barton and Zoback* [1992] found an exponent of 2.47 for more than 1600 aperture measurements on open fractures in core (apertures 2–9 cm), *Johnston and McCaffrey* [1996] found an exponent of 1.7–1.8 for veins (apertures 5–50 mm), and for 444 measurements of apertures on open fractures, *Barton* [1995b] found an exponent of 1.53 (apertures 1–10 mm). On the micron scale, *Belfield and Sovitch* [1995] obtained exponents of 2–2.4 (apertures 6–40 μm), and from an analysis of microcracks in granite and quartzite, *Wong et al.* [1989] found an exponent of 1.8 (apertures 3×10^{-2} to 10 μm). *Belfield* [1994] proposed that apertures of open fractures in core on the scale of millimeters were multifractal. Later, *Belfield* [1998] proposed that fracture apertures follow a Lévy stable distribution characterized by an index $\alpha = 1.85$, which is similar to the exponent of the power law tail of this distribution. These estimates of the aperture distribution exponent cover a wide range from 1.5 to 2.5.

Using the same simplification used in (21) and (22) for displacement (assuming perfect positive correlation), aperture may be related to fracture length by

$$A = \delta l^{n_2}, \tag{25}$$

where n_2 varies between 0.5 and 2 [*Stone*, 1984; *Vermilye and Scholz*, 1995; *Hatton et al.*, 1994; *Johnston*, 1994; *Walmann et al.*, 1996; *Renshaw and Park*, 1997]. Similarly to the displacement-length exponent n_1, variations in the exponent n_2 are due, in part, to interactions between fractures and, particularly, connectivity. Single isolated veins appear to give a linear relation with $n_2 = 1$ [*Stone*, 1984; *Vermilye and Scholz*, 1995], but more complex systems exhibit nonlinear relationships. *Vermilye and Scholz* [1995] have shown that for "en echelon" arrays of veins, the exponent is around 0.5. This agrees with the experimental results of *Walmann et al.* [1996], who found that for large deformations, $n_2 = 0.47$. In addition to these "sublinear" ($n_2 < 1$) relationships, "superlinear" relationships ($n_2 > 1$) may also exist. *Hatton et al.* [1994] and *Renshaw and Park* [1997] found for fissures in volcanic rocks of Iceland a characteristic length scale L_0 exists at 12 m, below which $n_2 \approx 3/2$ and above which $n_2 \approx 2/3$. This characteristic length scale L_0 is thought to reflect the onset of interactions between cracks at the critical crack density $\mathcal{P}$ [*Renshaw and Park*, 1997; *Main et al.*, 1999].

6.5. Variations in Fracture Property Exponents

Power laws appear to be good models for length, displacement, and aperture distributions of many fracture populations. However, there exist populations where other distributions (lognormal, exponential, and so forth) provide better fits to the observed data. Particularly for joint systems, the length distribution depends on the nature of layering [*Odling et al.*, 1999] where a lognormal distribution is most appropriate for joints confined to a single layer (stratabound systems) and a power law is appropriate for joints in more massive rocks (nonstratabound systems).

As discussed in sections 2.4 and 5, there are a number of problems associated with estimating power law exponents for fracture property data especially in the case of the commonly used cumulative distribution. These effects can be expected to give rise to uncertainties in the estimated exponents of perhaps as much as ±0.5. However, the observed range of exponents for fracture length populations (1.3–3.4) is much greater than this and is therefore likely to represent underlying physical influences on length exponents.

Joints and faults develop under different types of stress systems and they can often be distinguished geometrically, as the spatial organization of joints is generally more homogeneous than faults (see sections 4 and 7). Thus it might be expected that they would display distinct length exponents. However, from the plots of exponents in Figures 11 and 12, no clear distinction can be seen and both joint and fault systems display exponents covering the full range. The length distribution exponent thus appears, from the data in the literature, to be insensitive to the fracture type. However, on a plot of power law constant α versus exponent a (Figure 13c), joint and fault systems appear to form separate trends. Since α is representative of fracture density, this shows

that for a given exponent the joint systems tend to be denser than fault systems.

Physical experiments and numerical simulations of fracture system growth (sections 6.1 and 6.2) suggest that the power law exponent a approaches 2.0 as the fracture system develops with increasing strain, although the rate at which this occurs depends on many factors, such as material properties, structure, and water content of the rocks. This is consistent with a concept of universality for fracture systems, i.e., that the power law exponent converges on a value of 2.0 with increasing system maturity. Power law exponents from the literature (Figure 12), however, show a wide range of values, from 1.7 to 2.75. Following the results from experiments and simulations, this could suggest that natural systems display a range of maturity states. At the present time, however, there is no independent way of measuring the "maturity" of natural systems.

There are far fewer data sets on 2-D displacements and fracture apertures than on fracture lengths. The exponents tend to cover slightly narrower ranges than the length exponents but center on the same average values close to 2.0. Length-displacement and length-aperture relationships also seem to be power law. The exponents in these relationships, however, are not unique, and a range from superlinear to sublinear exists. Thus a full characterization of a fracture system requires the analysis of all attributes independently.

7. SYNTHESIS OF MEASUREMENTS ON FRACTAL DIMENSION

Numerous studies have investigated the fractal nature of fracture networks at various scales and report a wide range of fractal dimensions that for 2-D networks cover the range of theoretically possible values from 1 to 2. A list of fractal dimensions and their source articles is given in Table 4. Studies claim that fracture networks are fractal, with very few exceptions. There are two possible causes for the wide variation in reported fractal dimensions. These are, first, that results are inaccurate due to improper use of methods or that an insufficient number of fractures have been sampled, and second, that the variation is real and reflects underlying physical processes. For 2-D data sets, most studies have used the standard box-counting method or a modification of it, while a few studies have used the two-point correlation function.

7.1. Two-Dimensional Measurements

The most extensive study is that of *Barton* [1995a], who analyzed 17 fracture network maps at different scales. He gives an interesting account of the difficulties in estimating the fractal dimension of three fracture patterns from Yucca Mountain, Nevada, using the box-counting method. The initial analysis gave fractal dimensions from 1.12 to 1.16 [*Barton and Larsen*, 1985]. After reanalysis with a different range of cell sizes where care was taken to count only the minimum cells necessary to cover the fracture patterns, a range from 1.5 to 1.9 was found [*Barton et al.*, 1986; *Barton and Hsieh*, 1989]. A third analysis was carried out using a larger number of cell sizes (instead of multiples of 2) which gave a range of 1.38–1.52 [*Barton*, 1995a]. *Berkowitz and Hadad* [1997] reanalyzed the same 17 maps of *Barton* [1995a] also using the box-counting method but after cropping the maps to avoid problems with irregular boundaries and obtained fractal dimensions of 1.71–1.98. These estimates (1.12–1.98) cover nearly the whole range of possible values and illustrate that great care is required to obtain accurate results. For the final results from the 17 maps of 1.3–1.7 [*Barton*, 1995a], it was suggested that there is an increase in the fractal dimension with the addition of each successive generation of fractures. However, it can be seen that the fractal dimension estimates obtained show a positive correlation with the number of fractures in the sample up to a certain density, after which the estimate is stable. This effect has also been reported by others [*Barton*, 1995a; *Berkowitz and Hadad*, 1997] and probably indicates insufficient sampling of fractures in the less dense fracture patterns.

Gillespie et al. [1993] made an in-depth study of fault and joint data sets using the box-counting technique. For synthetic spatially random fracture patterns, they showed how the slope of the graph gradually evolves from 1 to 2 with increasing box size and thus represents a crossover between the topological dimensions of a single fracture (1-D) and the map (2-D). Similar results have been found for other natural fracture patterns [*Chiles*, 1988; *Odling*, 1992], and it was concluded that the box-counting method was not sensitive enough to distinguish between natural fracture systems and random distributions. A similar result was found [*Gillespie et al.*, 1993] using the fracture density technique [*LaPointe*, 1988].

The fractal nature of the San Andreas fault pattern has been much studied. *Aviles et al.* [1987] analyzed the roughness of the San Andreas fault at the continental scale and obtained dimensions of 1.008 and 1.0191, i.e., very close to the dimension of a straight line. *Okubo and Aki* [1987] studied the fault pattern in a 30-km-wide band around the San Andreas fault using the box-counting method and obtained fractal dimensions (D_0) of 1.12 and 1.43. Using the two-point correlation function on the southern part of the fault system with 3499 faults, *Bour and Davy* [1999] obtained a fractal dimension (D_2) of 1.65 defined by the variation in local slope over almost 2 orders of magnitude. The comparison of these three works is interesting because it illustrates how different results may be obtained on the same object depending on the scale of observation, the method used, and the type of fractal dimension.

Other estimates of fractal dimensions for fault systems include 0.85–1.4 for active fault systems in Japan and the Philippines [*Matsumoto et al.*, 1992], 0.7–1.6 for

TABLE 4. Compilation of Fractal Dimensions for Fracture Systems

Reference	*Type of Fractures*	*Size of the System, m*	*Method Used*	*Exponent*[a]
Aviles et al. [1987]	San Andreas fault	$\sim 3 \times 10^3$	box-counting	$D = 1.01$
Barton [1995] and *Berkowitz and Hadad* [1997]	joints	~15	box-counting	1.52 (B), 1.85 (BH)
	joints	~12		1.38 (B), 1.74 (BH)
	joints	~15		1.50 (B), 1.87 (BH)
	joints	~50		1.61 (B), 1.71 (BH)
	joints	~12		1.59 (B), 1.91 (BH)
	joints	~15		1.54 (B), 1.87 (BH)
	joints	~11		1.70 (B), 1.98 (BH)
	joints	~90		1.50 (B), 1.90 (BH)
	joints	~18		1.60 (B), 1.91 (BH)
	shear band	~1		1.50 (B), 1.89 (BH)
	...	~40		1.58 (B), 1.88 (BH)
	joints	~5		1.52 (B), 1.93 (BH)
	faults	$\sim 5 \times 10^3$		1.49 (B), 1.95 (BH)
	joints	~40		1.48 (B), 1.82 (BH)
	faults	$\sim 3 \times 10^3$		1.52 (B), 1.92 (BH)
	faults	$\sim 4 \times 10^6$		1.32 (B), 1.77 (BH)
	...	~0.02		1.58 (B), 1.88 (BH)
Bodin and Razack [1999]	...	$\sim 50 \times 10^3$	box-counting	$D_0 = 1.56$
			mass method	$D_M = 1.52$
Bour and Davy [1999]	faults	$\sim 250 \times 10^3$	two-point correlation	$D_c = 1.65$
Cello et al. [1997]	faults	$\sim 15 \times 10^3$	box-counting	$D = 1.60$
Chiles [1988]	...	~10	box-counting	$D = 2$
Gauthier and Lake [1993]	faults	$\sim 10^4$	modified box-counting [from *LaPointe*, 1988]	$D = 2.53$
	faults	$\sim 10^4$		$D = 2.44$
	faults	$\sim 10^4$		$D = 2.20$
Gillespie et al. [1993]	faults	$\sim 38 \times 10^3$	box-counting and modified box-counting [from *LaPointe*, 1988]	results not distinguishable from random networks ($D = 2$)
	faults	~2		
	faults	$\sim 13 \times 10^3$		
	joints	15		
Hirata [1989]	faults	$\sim 25 \times 10^3$	box-counting	$D = 1.49$
	faults	$\sim 70 \times 10^3$		$D = 0.72$
	faults	$\sim 73 \times 10^3$		$D = 1.60$
	...	~0.6		$D = 1.49$
LaPointe [1988]	joints	3	modified box-counting	$D = 2.71$
	joints	15		$D = 2.51$
	joints	15		$D = 2.54$
	joints	20		$D = 2.69$
	joints	15		$D = 2.37$
Matsumato et al. [1992]	faults	$\sim 7 \times 10^3$	box-counting	$D = 1.05$
		$\sim 8 \times 10^3$		$D = 1.12$
		$\sim 10 \times 10^3$		$D = 1.18$
		$\sim 15 \times 10^3$		$D = 1.33$
		$\sim 7 \times 10^3$		$D = 1.23$
		$\sim 5 \times 10^3$		$D = 1.42$
		$\sim 9 \times 10^3$		$D = 1.21$
		$\sim 7 \times 10^3$		$D = 1.18$
		$\sim 5 \times 10^3$		$D = 1.15$
		$\sim 9 \times 10^3$		$D = 1.22$
		$\sim 2 \times 10^3$		$D = 0.85$
		$\sim 2 \times 10^3$		$D = 0.92$
		$\sim 2 \times 10^3$		$D = 0.95$
Odling [1992]	joints	18	box-counting	$D = 2$
Okubo and Aki [1987]	faults	$\sim 15 \times 10^3$	box-counting	$D = 1.12$
		$\sim 15 \times 10^3$		$D = 1.20$
		$\sim 15 \times 10^3$		$D = 1.25$
		$\sim 15 \times 10^3$		$D = 1.21$
		$\sim 15 \times 10^3$		$D = 1.42$
		$\sim 15 \times 10^3$		$D = 1.43$
		$\sim 15 \times 10^3$		$D = 1.31$

Table 4. (continued)

Reference	*Type of Fracture*	*Size of System, m*	*Method Used*	*Exponent*
Walsh and Watterson [1993]	joints	~11	box-counting	$D = 2.00$
Multifractal analysis				
Agterberg et al. [1996]	faults and joints	~450		$D_0 = 1.98, D_2 = 1.93$
Giaquinta et al. [1999]	faults	$\sim 30 \times 10^3$	correlation function	$D_0 = 1.76, D_2 = 1.65$
	faults	$\sim 7 \times 10^3$		$D_0 = 1.67, D_2 = 1.56$
	faults	$\sim 7 \times 10^3$		$D_0 = 1.57, D_2 = 1.45$
Ouillon et al. [1996]	joints	10		$D_0 = 2.0, D_2 = 2.0$
	joints	60		$D_0 = 2.0, D_2 = 2.0$
	faults	11×10^3		$D_0 = 2.0, D_2 = 2.0$
	faults	45×10^3		$D_0 = 2.0, D_2 = 1.88$
	faults	150×10^3		$D_0 = 2.0, D_2 = 1.89$
Vignes-Adler et al. [1991]	faults	$\sim 1 \times 10^6$	mass method	$D_M = 1.97$
			box-counting	$D_0 = 2.0$
		$\sim 250 \times 10^3$	box-counting	$D_0 = 1.65$
		$\sim 40 \times 10^3$	box-counting	$D_0 = 2.00$
		$\sim 10 \times 10^3$	box-counting	$D_0 = 2.00$
		$\sim 100 \times 10^3$	box-counting	$D_0 = 2.00$
		$\sim 30 \times 10^3$	box-counting	$D_0 = 1.47, D_2 = 1.47$
		$\sim 22 \times 10^3$	box-counting	$D_0 = 1.48$
		$\sim 5.5 \times 10^3$	box-counting	$D_0 = 1.43, D_2 = 1.46$
		$\sim 5.5 \times 10^3$	box-counting	$D_0 = 1.36, D_2 = 1.46$
		$\sim 5.5 \times 10^3$	box-counting	$D_0 = 1.55, D_2 = 1.46$
		$\sim 5.5 \times 10^3$	box-counting	$D_0 = 1.48, D_2 = 1.46$

Only values measured on two-dimensional fracture networks have been reported.
[a] B means from *Barton* [1995a], BH means from *Berkowitz and Hadad* [1997].

faults in Japan [*Hirata*, 1989], and 1.64 for a fault array (lengths greater than 635 m) in the central Apennines, Italy [*Cello*, 1997]. *Vignes-Adler et al.* [1991] analyzed the fractal properties of fault patterns mapped from images at different scales that gave dimensions from 1.4 to 1.5. *LaPointe* [1988] measured the fractal dimensions of two-dimensional outcrop maps using an adapted three-dimensional box-counting method and obtained dimensions from 2.4 to 2.7. Also using this method, *Gauthier and Lake* [1993] found dimensions from 2.15 to 2.46 for different fracture orientation sets of faults in the North Sea (3-D seismic data).

Figure 16 shows a compilation of fractal dimensions from 2-D fracture patterns reported in the literature. This shows that fractal dimensions cover the theoretically possible range from 1.0 to 2.0 (reported values greater than 2 or less than 1.0 have not been included). The histogram in Figure 16b shows two peaks at fractal dimensions of 1.5 and 2.0. Fracture patterns with dimensions of 2.0 are not fractal, so fractal dimensions appear to cluster around a value of 1.5. It is presently unclear whether this represents a true fractal dimension or simply problems with application of the analysis techniques. The size of the maps on which the fractal analyses have been performed (Figure 16a) shows clearly that joint patterns come from the scale ranges of outcrop maps (1–100 m), while faults come from the scale range of regional maps, aerial photographs, and satellite images (1–100 km). Most fractal dimensions come from faults systems, in a fashion similar to the numbers of reported length exponents (section 6).

Only a few multifractal analyses on fracture patterns have been performed. *Ouillon et al.* [1996] analyzed several joint and fracture patterns at different scales from the sedimentary cover of Saudi Arabia. The highest-resolution data sets were found to be not fractal, but for the low-resolution maps (faults), generalized dimensions D_q varied from 2 to 1.6 as q evolved from 0 to 5. *Agterberg et al.* [1996] obtained similar variations in generalized dimensions for a fracture data set. *Berkowitz and Hadad* [1997] tested the multifractality of the 17 fracture maps of *Barton* [1995a] but found that their results were indistinguishable from those of synthetic data sets known not to be fractal. In general, multifractal measures are related to the study of a distribution of physical or other quantities on a geometric support [*Feder*, 1988]. In the case of fracture networks, this method has been mainly applied to describe the geometric support itself, which may explain the low variations of the generalized dimensions D_q. An additional problem arises with the statistical relevance of the analyses, as, for large q, the multifractal analysis examines the scaling properties of the densest areas of fracture networks only.

7.2. One-Dimensional Measurements

There are a large number of studies that have analyzed the scaling properties of one-dimensional fracture data sets. Two methods, the cantor dust, or interval

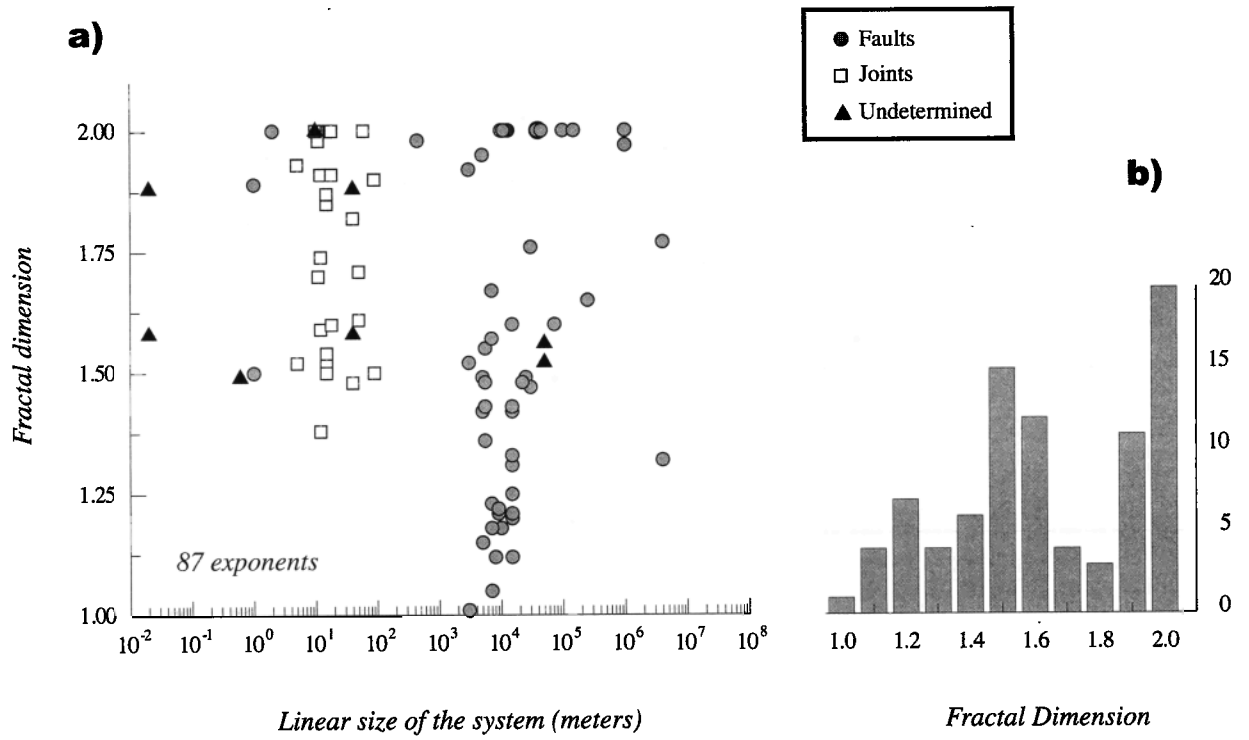

Figure 16. (a) Compilation of fractal dimensions reported in the literature as a function of the approximate linear size of the fracture networks. Only values measured on two-dimensional fracture networks have been reported. Reported values smaller than 1 and larger than 2 have been excluded. Note that fault networks are sampled mainly at kilometer scale, while joint networks are sampled mainly at outcrop scale. (b) Histogram of fractal dimensions. Although there is a large scatter, the histogram seems to show two peaks at $D = 2.0$ (nonfractal patterns) and $D = 1.5$.

counting, method (a one-dimensional analogue of the two-dimensional box-counting technique), and the spacing interval method, have been used. The cantor dust method has been applied to fracture data sets with scales from centimeters to kilometers [*Velde et al.*, 1990, 1991, 1993; *Merceron and Velde*, 1991; *Ledésert et al.*, 1993a, 1993b], giving dimensions generally around 0.3. In theory, for a fractal data set, the cumulative number of spacings greater than s should follow $C(s) \approx s^{-D}$, where D is the fractal dimension, while random spacings will result in a negative exponential distribution, and a Kolmogorov process will result in a lognormal frequency distribution [*Harris et al.*, 1991]. Using this method, *Gillespie et al.* [1993] found that joint networks were not fractal while fault networks frequently were, showing dimensions between 0.4 and 1.0. However, *Ouillon et al.* [1996] used the same method for analyzing a transect of about 600 joints and found a well-defined power law with an exponent of 0.5. Other fracture data sets have been found to show negative exponential distributions indicative of random spacing [*Brooks et al.*, 1996; *Genter and Castaing*, 1997; *Genter et al.*, 1997; *Odling et al.*, 1999].

7.3. Accuracy of Fractal Dimension Estimations

The large number of studies of the fractal nature of fracture networks suggests that natural fracture systems may be fractal, multifractal, or nonfractal. It is clear from the example of the patterns of *Barton* [1995a] that there exists a considerable problem associated with the estimation of fractal dimensions. As we have outlined in section 5, the main conditions that must be fulfilled to ensure accurate estimates are that the network must contain a sufficient number of fractures and that the scale range over which the dimension is estimated should show a generally constant value of local slope. Most of the results obtained on reliable 2-D data sets (i.e., with more than 1500 fractures) give dimensions close to 2 [*Odling*, 1992; *Ouillon et al.*, 1996; *Berkowitz and Hadad*, 1997], implying a homogeneous filling of the space, and are therefore nonfractal. The only studies that meet the previous criteria and that report lower dimensions around 1.7 are those from *Barton* [1995a], *Ouillon et al.* [1996], and *Bour and Davy* [1999]. However, the results of *Barton* [1995a] were revisited by *Berkowitz and Hadad* [1997], who found higher dimensions. *Ouillon et al.* [1996] analyzed the multifractal spectrum of several joint and fault patterns mapped at different scales. They found that the smaller-scale fracture patterns were not fractal, with all D_q equal to 2. However, data sets from large-scale fracture maps were multifractal, with D_q varying slightly from 2.0 to 1.6 for q of 0–5 [*Ouillon et al.*, 1996]. The results of *Bour and Davy* [1999] were obtained for the spatial distribution of

fault barycenters rather than fault traces, for which a higher dimension was obtained [*Bour*, 1997].

For most studies the fractal dimensions were derived on scale ranges of only 1 order of magnitude, mainly because of practical limitations on the scale range over which data can be collected. A simple estimate of the number of fractures that should be sampled can be made by integrating the density distribution between the smallest and largest fractures expected. In this way, it can be calculated that for $D = 1.7$, more than 100,000 fractures would be required to give a scale range for the estimation of the fractal dimension of 3 orders of magnitude, which is clearly impossible in practice. One way to overcome this difficulty is to work on fracture patterns mapped at different scales from the same locality, for example, the study of the fracture system of the Arabian Platform by *Ouillon et al.* [1996], who found that the system was multifractal. There are, however, still unresolved questions on how measurements made at different scales should be linked (see section 5.3).

It seems that the box-counting method should be used with caution because it does not appear to discriminate between natural fracture systems and spatially random patterns. However, it seems that the scaling properties of fault traces estimated by the box-counting method may be systematically different from that estimated using the two-point correlation function on fault barycenters [*Davy et al.*, 1990; *Bour and Davy*, 1999]. Studies on the properties of different fractal analysis techniques, and their sensitivity to the spatial distribution in natural fracture systems, are needed.

8. CONSEQUENCES AND DISCUSSION

This review has highlighted several issues regarding our present knowledge of the scaling properties of fractures. Given the quantity of literature on the subject, it may come as a surprise to some that even the basic fractal nature of fractures has not been established as rigorously as for many applications outside solid Earth geophysics. For example, from Figures 12 and 16 we can see that it is not at all unusual in the literature to find measurements of power law exponents and fractal dimensions of fracture populations based on data with a bandwidth of less than 1 order of magnitude of observation. This contrasts with the establishment of fractal dimensions in clouds in the atmosphere being measured over a scale range of 10^{-3}–10^{6} m in meteorology, some 9 orders of magnitude [*Lovejoy and Schertzer*, 1991]. In fact, far from highlighting "advances" in knowledge of the scaling properties of fractures, we have emphasized some of the outstanding problems that still remain in establishing the scaling properties of natural fractures. Some of these are inherent in making the primary observations, some are potentially solvable with a careful evaluation of the data, and some raise consequent questions in the form of other physically valid distributions that may describe the data. Here we break down some of these issues individually into the following classes: bandwidth of observation (sampling and truncation effects); nonfractal scaling due to characteristic size effects; clustering (correlation and self-organization); orientation distribution (fracture anisotropy); dimensionality of observation; and fracture type (shear or tensile displacement). We then go on to discuss possible future directions of research.

8.1. Scale Range of Observation

The most important issue in scaling is the determination of properties over as broad a scale range (bandwidth) as possible. For example, a common brief definition of a fractal set is one "with no characteristic length scale." However, *Mandelbrot* [1982] stated clearly that such a definition could not apply to natural fractal sets, since these all must have natural upper and lower limits. In his example a star may be a dominant volumetric object at close range, but recedes into being only one particle in a cloud of "dust" when examined on a galactic scale. At different scales, we therefore expect different dimensionalities as the norm, not the exception. Thus the primary question is, Is the data set fractal, within the bandwidth of observation?

As we have seen, we often cannot get a definitive answer to this question with many of the data sets available to us. However, this primary question is rarely posed a priori, i.e., before estimations of scaling exponents are determined. In fact, alternative explanations are commonly not even considered, far less eliminated, as possible descriptions of the data, and the narrower the bandwidth, the harder it is to be sure which of the potential distributions gives the best fit to the data. It is not an exaggeration to say that the application of fractal analysis to Earth science has often failed to match the rigor of initial applications in the primary references from other scientific disciplines.

One practical reason for this is the bandwidth of fractures available to us at outcrop. Good exposures of the rock surface are limited in extent and fractures may be degraded by erosion and/or chemical interaction, to the point where complete sampling is not possible. In layered sequences, fractures may be limited to particular horizons by the blunting effect of the stiffness contrast between neighboring beds [*Hobbs*, 1967] and so may be missed if not exposed. Often we only have one-dimensional (borehole) or two-dimensional (map) data, which may significantly undersample or oversample fracture density due to the location of the particular transect.

For example, *Berkowitz and Adler* [1998] discuss the resulting nonuniqueness of 3-D "reconstructions" of fracture network geometry, on the basis of 2-D maps. Three-dimensional seismic surveys and studies of serial sectioning at quarry faces can be used to assess the true 3-D structure, but at present, such data sets rarely provide enough information for robust statistical analysis.

All of these factors affect how representative the sample is that we have taken.

Even if we have 100% representative exposure, we are then left with establishing a reasonable minimum and maximum size for the Euclidean box within which the data will be analyzed (the arbitrary boundaries of the map). We have shown that even this first step may involve severe censoring effects, notably causing the systematic underestimation of the size of fracture traces larger than the box size. Similar artifacts can be introduced merely through the process of digitization and choosing the location and orientation of the primary "box" in box-counting algorithms for measuring fractal dimension [*Gonzato et al.*, 1998]. That is, the variability due to these "hidden," subjective, a priori constraints may introduce a sample bias comparable in size to the expected physical variability in scaling exponents.

Although these artifacts can be corrected to some extent by the methods summarized here (section 5), the censoring effects require knowledge from a scale larger than the box analyzed, reinforcing the necessity for broad bandwidth primary observation. Only when such effects are corrected can we begin to examine the causes for variations in power law exponents or the possible physical causes for any deviations from power law scaling, for example, due to bedding thickness, or rate processes such as the balance between boundary and local deformation (moment tensor) rates, as discussed below.

8.2. Nonfractal Scaling Due to Characteristic Size Effects

Before deciding on the best method for measuring the appropriate fractal dimension or power law scaling exponent, it is important to first put at risk the possibility that the data can best be described by a fractal set. This requires the elimination of other plausible, physically based forms for the distributions, as described below. A general power law frequency distribution $n(w)$ for a scale-invariant population is defined between two limits, $w_{\min}$ and $w_{\max}$, which represent the bandwidth of observation. Here w may be the length (equation (6)) displacement, aperture, or spacing, for example. This distribution has two free parameters, the density term α and the exponent a. Before fitting such a curve to data, we should also eliminate alternative possibilities. Other distributions that have been used to describe the distribution of fracture populations include the lognormal, or the exponential laws (section 2, equations (1) and (2)). These equations also have two free parameters. We may therefore choose objectively between them simply by comparing the residual sum of squares for the best fitting model parameters. Such an exercise is rarely undertaken, despite the fact that if we take an ideal lognormal distribution (equation (1)) and add a small amount of random noise, which we might expect with any finite sample, it can look surprisingly like a power law for sizes above $\langle w \rangle$. (The reader is encouraged to try this exercise as a tutorial.) It is therefore particularly important to establish whether or not the lower bound to fractal behavior is due to observational constraints ($w_{\min}$ above the true minimum) or a real characteristic size effect ($w_{\min}$ below the true minimum). Quite often, the fractal bandwidth for the curve fit is decided on by assuming a power law a priori, even though this implicit circular logic may obscure true characteristic size effects of the form of (1). These may remain even more hidden if the whole data set, i.e., including those points not used in the ultimate line fit, is not plotted. We conclude that no data filtering should be applied in plotting the distributions, so that the reader is free to make an independent judgement of the appropriate bandwidth and type of distribution.

Finally, characteristic size effects can be introduced not only through censoring effects on a large scale, but also due to the finite correlation length of any natural object or population. In percolation theory [e.g., *Stauffer and Aharony*, 1994], and in the physics of critical point phenomena [*Yeomans*, 1992], the general distribution of object size or spacing may take the form of a gamma distribution (equation (3)). This law reduces to the form of a power law when the characteristic length w_0 is much greater than $w_{\max}$. It also behaves very similarly to the finite size effect highlighted in this paper, due to fractures greater than the size of the box under investigation. Thus again it is important to have observations over a broad enough bandwidth to determine whether any exponential decline in frequency at large scales is due to a real correlation length or to an artificial finite size effect.

Finally, it has been suggested that there may be separate regions of behavior of the form of (4), requiring an extra two parameters:

$$\begin{aligned} n(w) &= \alpha_1 w^{-a_1} \qquad w_{\min} < w < w_c \\ n(w) &= \alpha_2 x^{-a_2} \qquad w_c < w < w_{\max}, \end{aligned} \tag{26}$$

where w_c is a characteristic length where the scaling exponent changes. Such behavior has been described for fracture systems by *Hatton et al.* [1994] and *Ackermann and Schlische* [1997] and for earthquake cumulative frequency data by *Triep and Sykes* [1997]. Here we have highlighted the importance of specifying when incremental or cumulative data are used and have shown that cumulative data are much more susceptible to finite size effects.

Assuming ideal sampling, it is straightforward to evaluate which distribution fits the data better, by minimizing the residual sum of squares. Alternatively, the data can be tested for fit to the different distribution types using the maximum (log) likelihood method [*Kagan*, 1991]. However, equation (3) requires three free parameters, and (26) requires four. If either is to be preferred, they have to outperform (4), (2), and (1) using a maximum likelihood method, which penalizes the additional degrees of freedom introduced by the greater number of model parameters, for example, Akaiki's or Schwartz's information criteria, as appropriate [*Main et al.*, 1999].

8.3. Clustering

We have seen that the spatial correlation of fractures is of prime importance in determining their geometrical properties and hence has consequences for fracture evolution or transport properties. It is important to emphasize that a random process also has clustering properties, so as a first step we have to demonstrate clustering above (or below) that predicted by a Poisson process [*Turcotte*, 1992]. In most geological applications, the preferred method is the use of the correlation integral, which applies to a set of points [*Grassberger and Procaccia*, 1983]. For fractures this requires a reduction of a set of traces, with variable offset along strike, to a set of points. The first step is to untangle intersecting traces, since T and Y junctions abound, particularly in the case of joints. In addition, apparently disconnected fractures in 2-D may be connected in 3-D at depth. This introduces a fundamentally subjective step in the data analysis not present for, say, earthquake hypocenter data. The second step is then to reduce the spatial information to a point, for example, the center of mass, or "barycenter." Again it is important to determine objective and consistent methods of reducing the data to a set of points before calculating the correlation integral, while bearing in mind that this simplification involves the loss of what may be critical information on the finite length and orientation of the fracture traces.

The issue of bandwidth is also important here, since in the original paper [*Grassberger and Procaccia*, 1983] some 4 orders of magnitude were required before the characterization of a dynamic attractor in phase space could be deemed "strange" (i.e., fractal). One of the consequences of such a broadband treatment is to minimize finite size effects, which occupy a smaller part of the curve. The very narrowband determination of the correlation dimension, common in the literature, is another case where clear caveats in the primary reference have often been ignored in subsequent application.

It is therefore important to evaluate alternative methods of analyzing the clustering properties, including methods based on weighted (mass) fractals, or their generalization to multifractals. It is also important to evaluate the possibility of other potential forms for the correlation function, i.e., that of (3) for systems near the percolation threshold.

8.4. Dimensionality

The dimensionality of the measurements is a serious limitation in determining the true scaling exponents in surface maps or borehole samples. To correct for this known effect, it is common in the literature to correct for 2-D sampling, using

$$\xi_{3D} = \xi_{2D} + 1, \tag{27}$$

where ξ_{3D} is the true (3-D) scaling exponent and ξ_{2D} is the exponent for the 2-D sample. This equation apparently corrects for dimensional sampling effects. However, this holds only for a well-sampled, representative population of fractures with random orientations and with a uniform spatial distribution. It therefore does not necessarily hold for fracture sets with strong spatial correlation and clustering (either fractal or characteristic) or with strong directional anisotropy, both common observations in fracture statistics. A more appropriate relationship has the form [*Borgos et al.*, 2000; *Hatton et al.*, 1993]

$$\xi_{3D} = A \times \xi_{2D} + B, \tag{28}$$

where $A = 1.28$ and $B = -0.23$ [*Hatton et al.*, 1993]. We conclude that if (27) is used, the observation of randomly oriented, well-sampled fractures must first be demonstrated independently. This problem is likely to be even more severe when estimates are based on 1-D borehole data.

We have not discussed the effect of orientation in detail, even though it impacts strongly on two critical issues, namely, the probability of fractures intersecting both each other (in terms of spatial correlations) and the surface of measurement. The orientation of the Euclidean box relative to the predominant strike of the objects can also exert a strong hidden control on estimates of the fractal (box-counting) dimension [*Gonzato et al.*, 1998]. Elsewhere in this review we have highlighted many similarities between faults and joints. However, one of the main differences in terms of fracture trace maps may be the orientation distribution, due to the systematic differences in the stress field at crack tips in either case. Such differences may or may not feed through into differences in scaling exponents or the probability of exposure on a mapped surface. The issue of orientation also affects the estimation of scaling exponents, since it determines the probability of intersection of fracture traces with the measured surface, which may or may not be oblique to the fracture orientation. Very few studies have explicitly addressed the effect of orientation on determination of scaling exponents.

8.5. Fracture Type

Both faults and joints show a wide range of power law exponents for fracture length, displacement, and aperture (section 6). Errors of estimation for the exponents may explain part of this variation, but is not thought sufficient to account for the full range of values. A possible underlying physical cause for this variation may be the "maturity" of natural systems. Physical experiments and numerical simulations suggest that length exponents converge on a value of around 2.0 as the fracture system develops. It can be expected that natural systems show a range of maturity levels and thus a range of exponent values.

We have shown that some scaling exponents (notably, the length distribution exponent) are remarkably insensitive to the orientation of the slip vector, i.e., whether or not fracturing is accompanied by shear (faults) or tensile

(joints) displacement. In fact, it is rather hard to pin down what the quantitative difference between the two failure mechanisms is using scaling exponents alone, despite the relative ease with which this can be done with the experienced eye of a field geologist. Part of the reason for this may be that these differences show up in complex positional and directional arrangements reflected more in the "spatial phase" (absolute position) than the "amplitude" distribution measured in traditional scaling exponents. A potential example of this is the subtle interplay of stress fields that leads to the common occurrence of T and Y junctions in joint sets, requiring the simultaneous occurrence of position, orientation, and relative size constraints during their formation. Another example is the stress rotation effects caused by fracture interactions and stress relaxation [*Simon et al.*, 1999]. Such effects are hard to capture with traditional scaling analysis which decouples such effects into individual components.

The concept of spatial phase is also important in any reconstruction of synthetic fracture sets. However we characterize the set, and constrain with available map data, we can never predict exactly where a fracture or fracture cluster will actually be in the subsurface. Scaling is always to some extent a statistical (stochastic) issue and can be addressed most appropriately to problems where a spatial average, rather than the location of individual fractures, is of primary importance.

8.6. Future Research

The discussion above clearly highlights the need for an improved "arsenal" of geological and geophysical techniques (including tomography, ground-penetrating radar, and so forth) to improve on the quality and relevance of the data available to us, particularly in 3-D. There are severe practical difficulties in extending the scale range of observations in order that exponents may be determined over 2–3 orders of magnitude. A promising way of overcoming this difficulty is by compilations of data sets, of the same fracture system, at a range of scales and resolutions. The manner in which such data sets should be combined, however, requires further investigation. It is also clear that we require improved rock fracture models to take account of the subtle spatial relationships between fractures in a population and to test potential methods of characterizing such relationships under known model conditions. We also need to resolve the debate about what parameters best characterize the geometrical structure and scaling properties of fracture systems and whether they are or should be different for joints and faults.

In particular, this review has highlighted the basic need to pose the scaling hypotheses to be tested (and put at risk) more objectively than is commonly the case, before searching for answers and deciding what kind of analysis to perform. Many unresolved issues remain, including finding objective ways to analyze simultaneously for orientation and spatial position; quantifying the spatial correlation of objects with finite length (as the linearity of fractures is really a key feature); and forming better understanding of physical controls on growth processes in populations of fractures.

Finally, even if such questions could be overcome in principle, solving for the scaling parameters discussed here is not sufficient on its own to characterize the flow of fluids or the transport of contaminants/chemicals in fracture networks. This would require additional information on the structure, hydrodynamics, and pressure-sensitive chemical properties of individual fractures.

9. CONCLUSIONS

The scaling properties of fracture populations can in principle be determined quantitatively by methods developed in other disciplines to describe the geometrical properties of nonlinear systems. In particular, much use has been made of fractal scaling, but this hypothesis is seldom put at risk a priori before drawing important conclusions of the implications for applications to fracture growth mechanics or contaminant dispersion. We conclude that as a matter of routine, other physically valid distributions that may describe the data are eliminated before a fractal distribution is preferred.

The basic problem is that we are faced with a high degree of uncertainty in data; clearly, there is tremendous difficulty, and in some situations a virtual impossibility, in locating, measuring, and analyzing fractures in three dimensions in situ. Analyses are therefore usually based on measurements of fractures at outcrops, in core samples, and from various geophysical techniques, as well as on theoretical models of rock fracture; all of these studies must rely on extrapolation and subjective considerations. Some can be corrected for uniquely, notably, the effect of finite study area on the fault length distribution, but many potential sources of sample bias cannot be easily corrected for at present. These include effects of resolution (truncation) and extrapolation from 1-D and 2-D to 3-D exponents. The elimination of such artifacts, including sampling, truncation, and censoring effects, spatial correlation, and orientation anisotropy, is important because they may propagate into erroneous predictions for fluid flow and contaminant transport on a larger scale.

Fractal dimensions, in particular, are an appealing (and "fashionable") means to analyze fracture systems, but measurements of "fractal" dimensions are usually based on fracture data with a bandwidth of over less than 1 order of magnitude of observation. Moreover, it is now clear that fractal dimensions or scaling exponents on their own, even if they are "well defined," do not characterize the full structural pattern of fracture networks. On the other hand, fractal characterizations can be convenient, as well as useful, where they provide a better

description of the data than other plausible alternative distributions. By examining the literature, we find, for example, a wide range of power law exponents for the length distribution. There are probably both sampling and physical causes for this variation, but exponents concentrate around 2.0, irrespective of whether tensile or shear fractures are observed. For seismometers acting as velocity transducers, this result is consistent with the observed seismic b value of 1, implying that tensile fractures, faults, and earthquakes all have dimensions whose frequencies scale very nearly linearly with rupture area. The underlying cause for this apparent universality has yet to be explained.

GLOSSARY

Boudinage: A structure in which competent beds bounded by incompetent ones have been divided into segments during metamorphism and deformation.

Capacity dimension: The fractal dimension D_0, representing the spatial distribution of the unweighted measure of the object, determined by the box-counting method.

Correlation dimension: Fractal dimension D_2, estimated using the correlation function. This dimension describes how parts of the object are related to each other spatially. Theoretically, it corresponds to the weight measure, $q = 2$, describing the properties of multifractal set Dq (see capacity dimension).

Density constant, α: Constant in the power law density length distribution: $n(l) = \alpha l^{-a}$.

Exposure: Geological term describing rocks at the surface of the Earth's crust that are exposed to the atmosphere and available for observation.

Fault: A mode II fracture, i.e., a fracture displaying in-plane shear displacement.

Fractal: In theory, a fractal dimension is a noninteger topological dimension of the space that embeds an object with complex geometry ramified to infinitesimal details. A common brief definition of a fractal set is one with no characteristic length scale. However, *Mandelbrot* [1982] stated clearly that such a definition cannot apply to natural fractal sets, since these all must have natural upper and lower limits. Thus, for fractals in nature, the above definition applies only within a limited scale range.

Fracture: General term used to describe any discontinuity within a rock mass that developed as a response to stress.

Fracture density: Measure describing the number of fractures per unit area.

Information dimension: Fractal dimension D_1, representing the distribution of the object's mass and is a generalization of the capacity dimension. It corresponds to the weight measure $q = 1$ describing the properties of multifractal set Dq.

Joint: Mode I fracture, i.e., a fracture displaying displacement normal to the discontinuity walls.

Length exponent, a: Exponent of the power law fracture length density distribution: $n(l) = \alpha l^{-a}$. It determines the rate at which the frequency of fractures decreases with increasing length.

Mass dimension: Fractal dimension D_M, measured by counting the total mass of an object included in disks of radius r. This dimension is not necessarily equivalent to Dq ($q = 0, 1, 2, \ldots$).

Multifractal: A multifractal may be thought of as an interwoven set of fractals associated with an object. The fractal dimensions D_q ($q = 0, 1, 2, \ldots$) describe how the various moments of the object's "mass" distribution scale with volume considered.

Outcrop: Rocks occurring at the surface of the Earth's crust that may or may not be covered with superficial deposits (unconsolidated sediments and soil).

Scale invariance: A property of objects that show a similar appearance at all scales.

Self-similar: Term describing an object exhibiting isotropic scale invariance.

Universality: A property of different physical systems whose behavior nevertheless exhibits similarities. These take the form of similar scaling rules and scaling exponents (for parameters such as the order parameter or correlation length) near the critical point of the system.

Vein: Tabular mass of mineral matter, deposited in a fissure or crack in a rock, and differing in composition from the substance in which it is embedded.

ACKNOWLEDGMENTS. We thank the European Community for their financial support (contract ENV4-CT97-0456). We thank Scott Doney and Didier Sornette for their constructive criticism.

Jim Smith was the Editor responsible for this paper. He thanks two anonymous technical reviewers and one anonymous cross-disciplinary reviewer.

REFERENCES

Ackermann, R. V., and R. W. Schlische, Anticlustering of small normal faults around larger faults, *Geology*, *25*(12), 1127–1130, 1997.

Agterberg, F. P., Q. Cheng, A. Brown, and D. Good, Multifractal modeling of fractures in the Lac du Bonnet batholith, Manitoba, *Comput. Geosci.*, *22*(5), 497–507, 1996.

Anders, M. H., and D. V. Wiltschko, Microfracturing, paleostress and the growth of faults, *J. Struct. Geol.*, *16*, 795–815, 1994.

Atkinson, B. K. (Ed.), *Fracture Mechanics of Rocks*, Academic, San Diego, Calif., 1987.

Aviles, C. A., C. H. Scholz, and J. Boatwright, Fractal analysis applied to characteristic segments of the San Andreas fault, *J. Geophys. Res.*, *92*, 331–344, 1987.

Bahat, D., Jointing and fracture interactions in middle Eocene chalks near Beer-Sheva, Israel, *Tectonophysics*, *136*, 299–321, 1987.

Barton, C. A., and M. D. Zoback, Self-similar distribution and properties of macroscopic fractures at depth in crystalline rock in the Cajon Pass scientific drill hole, *J. Geophys. Res.*, *97*, 5181–5200, 1992.

Barton, C. C., Fractal analysis of scaling and spatial clustering of fractures, in *Fractals in the Earth Sciences*, edited by C. C. Barton and P. R. LaPointe, pp. 141–178, Plenum, New York, 1995a.

Barton, C. C., Bedrock geological map of Hubbard Brooks experimental forest and maps of fractures and geology in road cuts along Interstate 93, Grafton County, New Hampshire, *Rep. I-2562, U.S. Geol. Surv. Misc. Invest. Ser.*, 2 pp., 1995b.

Barton, C. C., and P. A. Hsieh, Physical and hydrological flow properties of fractures, *Field Trip Guidebook T385*, AGU, Washington, D. C., 1989.

Barton, C. C., and E. Larsen, Fractal geometry of two-dimensional fracture networks at Yucca Mountain, southwestern Nevada, in *Proceedings of the International Symposium on Fundamentals of Rock Joints*, edited by O. Stephannson, pp. 77–84, Centek, Luleå, Sweden, 1985.

Barton, C. C., C. B. Gott, and J. R. Montgomery, Fractal scaling of fracture and fault maps at Yucca Mountain, southern Nevada (abstract), *Eos Trans. AGU*, *67*(44), 1295, 1986.

Belfield, W. C., Simulation of subseismic faults using fractal and multifractal geometry, presented at the 67th Annual Technical Conference and Exhibition of the Society of Petroleum Engineers, Washington, D. C., Oct. 4–7, 1992.

Belfield, W. C., Multifractal characteristics of natural fracture apertures, *Geophys. Res. Lett.*, *21*, 2641–2644, 1994.

Belfield, W. C., Incorporating spatial distribution into stochastic modelling of fractures: Multifractals and Lévy-stable statistics, *J. Struct. Geol.*, *20*, 473–486, 1998.

Belfield, W. C., and J. Sovitch, Fractures statistics from horizontal wellbores, *J. Can. Pet. Technol.*, *34*, 47–50, 1995.

Berkowitz, B., and P. M. Adler, Stereological analysis of fracture network structure in geological formations, *J. Geophys. Res.*, *103*, 15,339–15,360, 1998.

Berkowitz, B., and A. Hadad, Fractal and multifractal measures of natural and synthetic fracture networks, *J. Geophys. Res.*, *102*, 12,205–12,218, 1997.

Blackstone, D. L., Jr., Traveller's guide to the geology of Wyoming, *Bull. Geol. Surv. Wyo.*, *67*, 130 pp., 1988.

Bodin, J., and M. Razack, L'analyse d'images appliquée au traitement automatique de champs de fractures, propriétés géométriques et lois d'échelles, *Bull. Soc. Geol. France*, *170*(4), 579–593, 1999.

Bonnet, E., La localisation de la déformation dans les milieux fragiles-ductiles: Approche expérimentale et application à la lithosphère continentale, Ph.D. thesis, 200 pp., Geosci. Rennes, Univ. of Rennes, Rennes, France, 1997.

Borgos, H. G., P. A. Cowie, and N. H. Dawers, Practicalities of extrapolating one-dimensional fault and fracture size-frequency distributions to higher-dimensional samples, *J. Geophys. Res.*, *105*, 28,377–28,391, 2000.

Bour, O., Transferts de fluides dans les milieux fracturés: Effets d'échelle, Ph.D. thesis, 288 pp., Geosci. Rennes, Univ. of Rennes, Rennes, France, 1997.

Bour, O., and P. Davy, Connectivity of random fault networks following a power law fault length distribution, *Water Resour. Res.*, *33*, 1567–1583, 1997.

Bour, O., and P. Davy, On the connectivity of three-dimensional fault networks, *Water Resour. Res.*, *34*, 2611–2622, 1998.

Bour, O., and P. Davy, Clustering and size distribution of fault patterns: Theory and measurements, *Geophys. Res. Lett.*, *26*, 2001–2004, 1999.

Brooks, B. A., R. W. Allmendinger, and I. Garrido de la Barra, Fault spacing in El Teniente mine, central Chile: Evidence for nonfractal fault geometry, *J. Geophys. Res.*, *101*, 13,633–13,653, 1996.

Burg, J. M., J. Martinod, and P. Davy, Buckling of the oceanic lithosphere from geophysical data and experiments, *Tectonics*, *11*, 537–548, 1992.

Carbotte, S. M., and K. C. McDonald, Comparison of seafloor tectonic fabric at intermediate, fast, and super fast spreading ridges: Influence of spreading rate, plate motions, and ridge segmentation on fault patterns, *J. Geophys. Res.*, *99*, 13,609–13,631, 1994.

Carter, K. E., and C. L. Winter, Fractal nature of normal faults in the Española basin, Rio Grande rift, New Mexico: Implications for fault growth and brittle strain, *J. Struct. Geol.*, *17*, 863–873, 1995.

Cartwright, J. A., B. D. Trugdill, and C. S. Mansfield, Fault growth by segment linkage: An explanation for scatter in maximum displacement and trace length data from the Canyonlands grabens of SE Utah, *J. Struct. Geol.*, *17*, 1319–1326, 1995.

Castaing, C., et al., Scaling relationships in intraplate fracture systems related to Red Sea rifting, *Tectonophysics*, *261*, 291–314, 1996.

Cello, G., Fractal analysis of a Quaternary fault array in the central Apennines, Italy, *J. Struct. Geol.*, *19*, 945–953, 1997.

Cello, G., L. Marchegiani, S. Mazzoli, and E. Tondi, Fractal analysis of the upper Quaternary faults in the central Appenines (in Italian), *Stud. Geol. Camerti*, *14*, 305–315, 1997.

Charlaix, E., E. Guyon, and N. Rivier, A criterion for percolation threshold in a random array of plates, *Solid State Commun.*, *50*(11), 999–1002, 1984.

Charmet, J. C., S. Roux, and E. Guyon (Eds.), Disorder and fracture, *NATO ASI Ser., Ser. B*, *235*, 305 pp., Plenum, New York, 1990.

Childs, C., J. J. Walsh, and J. Watterson, A method for estimation of the density of fault displacements below the limits of seismic resolution in reservoir formations, in *North Sea Oil and Gas Reservoirs II*, edited by A. T. Buller et al., pp. 309–318, Graham and Trotman, Norwell, Mass., 1990.

Chilès, J. P., Fractal and geostatistical methods for modeling of a fracture network, *Math. Geol.*, *20*, 631–654, 1988.

Cladouhos, T. T., and R. Marrett, Are fault growth and linkage models consistent with power-law distribution of fault length?, *J. Struct. Geol.*, *18*, 281–293, 1996.

Clark, R. M., and S. J. D. Cox, A modern regression approach to determining fault displacement-length scaling relationships, *J. Struct. Geol.*, *18*, 147–152, 1996.

Clark, R. M., S. J. D. Cox, and G. M. Laslett, Generalizations of power-law distributions applicable to sampled fault-trace length: Model choice, parameter estimation and caveats, *Geophys. J. Int.*, *136*, 357–372, 1999.

Cowie, P. A., Normal fault growth in three dimensions in continental and oceanic crust, in *Faulting and Magmatism at Mid-Ocean Ridges, Geophys. Monogr. Ser.*, vol. 106, edited by W. R. Buck et al., pp. 325–348, AGU, Washington, D. C., 1998.

Cowie, P. A., and C. H. Scholz, Physical explanation for the displacement-length relationship of fault using a post-yield fracture mechanics model, *J. Struct. Geol.*, *14*, 1133–1148, 1992a.

Cowie, P. A., and C. H. Scholz, Displacement-length scaling relationships for faults: Data synthesis and discussion, *J. Struct. Geol.*, *14*, 1149–1156, 1992b.

Cowie, P. A., C. Vanneste, and D. Sornette, Statistical physics model for the spatiotemporal evolution of faults, *J. Geophys. Res.*, *98*, 21,809–21,822, 1993a.

Cowie, P., C. H. Scholz, M. Edwards, and A. Malinverno, Fault strain and seismic coupling on mid-ocean ridges, *J. Geophys. Res.*, *98*, 17,911–17,920, 1993b.

Cowie, P. A., D. Sornette, and C. Vanneste, Multifractal scaling properties of a growing fault population, *Geophys. J. Int.*, *122*, 457–469, 1995.

Cox, S. J. D., and L. Paterson, Damage development during rupture of heterogeneous brittle materials: A numerical study, in *Deformation Mechanisms, Rheology and Tectonics*, edited by R. J. Knipe and E. H. Rutter, *Geol. Soc. Spec. Publ.*, *54*, 57–62, 1990.

Crave, A., and P. Davy, Scaling relationships of channel networks at large scales: Examples from two large-magnitude water-sheds in Brittany, France, *Tectonophysics*, *269*, 91–117, 1997.

Cruden, D. M., Describing the size of discontinuities, *Int. J. Rock Mech. Min. Sci. Geomech. Abstr.*, *14*, 133–137, 1977.

Dauteuil, O., and J. P. Brun, Deformation partitioning in a slow spreading ridge undergoing oblique extension: Mohns Ridge, Norwegian Sea, *Tectonics*, *15*, 870–884, 1996.

Davy, P., On the frequency-length distribution of the San Andreas fault system, *J. Geophys. Res.*, *98*, 12,141–12,151, 1993.

Davy, P., A. Sornette, and D. Sornette, Some consequences of a proposed fractal nature of continental faulting, *Nature*, *348*, 56–58, 1990.

Davy, P., A. Sornette, and D. Sornette, Experimental discovery of scaling laws relating fractal dimensions and the length distribution exponent of fault systems, *Geophys. Res. Lett.*, *19*, 361–363, 1992.

Davy, P., A. Hansen, E. Bonnet, and S. Z. Zhang, Localization and fault growth in layered brittle-ductile systems: Implications for deformation of the continental lithosphere, *J. Geophys. Res.*, *100*, 6281–6294, 1995.

de Arcangelis, L., and H. J. Herrmann, Scaling and multiscaling laws in random fuse networks, *Phys. Rev. B*, *39*, 2678–2684, 1989.

de Arcangelis, L., A. Hansen, H. J. Herrmann, and S. Roux, Scaling laws in fracture, *Phys. Rev. B*, *40*, 877–880, 1989.

Dershowitz, W. S., and H. H. Einstein, Characterizing rock joint geometry with joint system models, *Rock Mech. Rock Eng.*, *21*, 21–51, 1988.

Dyer, R., Using joint interactions to estimate paleostress ratios, *J. Struct. Geol.*, *10*, 685–699, 1988.

Einstein, H. H., and G. B. Baecher, Probabilistic and statistical methods in engineering geology, *Rock Mech. Rock Eng.*, *16*, 39–72, 1983.

Falconer, K., *Fractal Geometry: Mathematical Foundations and Applications*, John Wiley, New York, 1990.

Feder, J., *Fractals*, 283 pp., Plenum, New York, 1988.

Fossen, H., and J. Hesthammer, Geometric analysis and scaling relations of deformation bands in porous sandstone from the San Rafael Desert, Utah, *J. Struct. Geol.*, *19*, 1479–1493, 1997.

Frisch, U., and D. Sornette, Extreme deviations and applications, *J. Phys. I*, *7*, 1155–1171, 1997.

Gauthier, B. D. M., and S. D. Lake, Probabilistic modeling of faults below the limit of seismic resolution in Pelican field, North Sea, offshore United Kingdom, *Am. Assoc. Petrol. Geol. Bull.*, *77*, 761–777, 1993.

Genter, A., and C. Castaing, Effets d'échelle dans la fracturation des granites, *C. R. Acad. Sci., Ser. II Sci. Terr. Planet.*, *325*, 439–445, 1997.

Genter, A., C. Castaing, C. Dezayes, H. Tenzer, H. Traineau, and T. Villemin, Comparative analysis of direct (core) and indirect (borehole imaging tools) collection of fracture data in the Hot Dry Soultz reservoir (France), *J. Geophys. Res.*, *102*, 15,419–15,431, 1997.

Gertsch, L. S., Three-dimensional fracture network models from laboratory-scale rock samples, *Int. J. Rock Mech. Min. Sci. Geomech. Abstr.*, *32*, 85–91, 1995.

Gervais, F., and S. Genter, Tridimensional geometrical description of the fracture pattern of a stratified rock mass, in *Proceedings of the International Congress on Rock Mechanics*, edited by W. Wittke, Aachen, Germany, pp. 237–240, 1991.

Giaquinta, A., S. Boccaletti, M. Boccaletti, L. Piccardi, and F. T. Arecchi, Investigating the fractal properties of geological fault systems: The Main Ethiopian Rift case, *Geophys. Res. Lett.*, *26*, 1633–1636, 1999.

Gil, R. D., and S. Johansen, A survey of product integration with a view toward application in survival analysis, *Ann. Stat.*, *18*, 1501–1555, 1990.

Gillespie, P. A., J. J. Walsh, and J. Watterson, Limitations of dimension and displacement data from single faults and the consequences for data analysis and interpretation, *J. Struct. Geol.*, *14*, 1157–1172, 1992.

Gillespie, P. A., C. Howard, J. J. Walsh, and J. Watterson, Measurement and characterisation of spatial distribution of fractures, *Tectonophysics*, *226*, 113–141, 1993.

Gonzato, G., F. Mulargia, and W. Marzocchi, Practical application of fractal analysis: Problems and solutions, *Geophys. J. Int.*, *132*, 275–282, 1998.

Grassberger, P., Generalized dimensions of strange attractors, *Phys. Lett. A*, *97*, 227–230, 1983.

Grassberger, P., and I. Procaccia, Measuring the strangeness of strange attractors, *Physica D*, *9*, 189–208, 1983.

Griffith, A. A., The phenomena of rupture and flow in solids, *Philos. Trans. R. Soc. London, Ser. A*, *221*, 163–198, 1920.

Gross, M. R., The origin and spacing of cross joints: Examples from the Monterrey formation, Santa Barbara coastline, California, *J. Struct. Geol.*, *15*, 737–751, 1993.

Gross, M. R., G. Gutierrez-Alonzo, T. Bai, M. A. Wacker, K. B. Collinsworth, and R. J. Behl, Influence of mechanical stratigraphy and kinematics on fault scaling relations, *J. Struct. Geol.*, *19*, 171–183, 1997.

Gudmundsson, A., Tectonics of the Thingvellir fissure swarm, SW Iceland, *J. Struct. Geol.*, *9*, 61–69, 1987a.

Gudmundsson, A., Geometry, formation and development of tectonics fractures on the Reykjanes Peninsula, southwest Iceland, *Tectonophysics*, *139*, 295–308, 1987b.

Hakami, E., Aperture distribution of rock fractures, Ph.D. thesis, Dep. of Civ. and Environ. Eng., R. Inst. of Technol., Stockholm, 1995.

Hamburger, D., O. Biham, and D. Avnir, Apparent fractality emerging from models of random distributions, *Phys. Rev. E*, *53*, 3342–3358, 1996.

Hansen, A., E. L. Hinrichsen, and S. Roux, Scale invariant disorder in fracture related breakdown phenomena, *Phys. Rev. B*, *43*, 665–678, 1991.

Harris, C., R. Fransse, and R. Loosveld, Fractal analysis of fractures in rocks: The Cantor's Dust method—Comment, *Tectonophysics*, *198*, 107–115, 1991.

Hatton, C. G., I. G. Main, and P. G. Meredith, A comparison of seismic and structural measurements of fractal dimension during tensile subcritical crack growth, *J. Struct. Geol.*, *15*, 1485–1495, 1993.

Hatton, C. G., I. G. Main, and P. G. Meredith, Nonuniversal scaling of fracture length and opening displacement, *Nature*, *367*, 160–162, 1994.

Heffer, K. J., and T. G. Bevan, Scaling relationships in natural fractures: Data, theory, and application, in *Proceedings of the 2nd European Petroleum Conference*, pp. 367–376, Soc. of Pet. Eng., Richardson, Tex., 1990.

Henderson, J. R., C. MacLean, I. G. Main, and M. G. Norman, A fracture-mechanical cellular automaton model of seismicity, *Pure Appl. Geophys.*, *142*, 545–565, 1994.

Hentschel, H. G. E., and I. Proccacia, The infinite number of generalised dimensions of fractals and strange attractors, *Physica D*, *8*, 435–444, 1983.

Herrmann, H. J., and S. Roux (Eds.), *Statistical Models for the*

Fracture in Disordered Media, 351 pp., North-Holland, New York, 1990.

Heuze, F. E., Scale effects in the determination of rock mass strength and deformability, *Rock Mech.*, *12*, 167–192, 1980.

Hirata, T., Fractal dimension of fault systems in Japan: Fractal structure in rock fracture geometry at various scales, *Pure Appl. Geophys.*, *121*, 157–170, 1989.

Hobbs, D. W., The formation of tension joints in sedimentary rocks: An explanation, *Geol. Mag.*, *104*, 550–556, 1967.

Hudson, J. A., and S. D. Priest, Discontinuities and rock mass geometry, *Int. J. Mech. Min. Sci. Geomech. Abstr.*, *16*, 339–362, 1979.

Hudson, J. A., and S. D. Priest, Discontinuity frequency in rock masses, *Int. J. Mech. Min. Sci. Geomech. Abstr.*, *20*, 73–89, 1983.

Irwin, G. R., Plastic zone near a crack and fracture toughness, in *Proceedings of the 7th Sagamore Army Materials Research Conference*, edited by W. A. Backofen, IV-63, Syracuse Univ. Press, Syracuse, N. Y., 1960.

Jackson, P., and D. J. Sanderson, Scaling of fault displacements from the Badajoz-Cordoba shear zone, SW Spain, *Tectonophysics*, *210*, 179–190, 1992.

Johnston, J. D., Fractal geometries of filled fracture systems—Scaling of mechanism, in *Tectonic Studies Group Special Meeting, Edinburgh, October 19–20, Fault Population, Extended Abstract Volume*, pp. 64–66, Geol. Soc., London, 1994.

Johnston, J. D., and K. J. W. McCaffrey, Fractal geometries of vein systems and the variation of scaling relationships with mechanism, *J. Struct. Geol.*, *18*, 349–358, 1996.

Kagan, Y. Y., Seismic moment distribution, *Geophys. J. Int.*, *106*, 123–134, 1991.

Kagan, Y. Y., Seismic moment-frequency relation for shallow earthquakes: Regional comparison, *J. Geophys. Res.*, *102*, 2835–2852, 1997.

Kakimi, T., Magnitude-frequency relation for displacement of minor faults and its significance in crustal deformation, *Bull. Geol. Surv. Jpn.*, *31*, 467–487, 1980.

Kanamori, H., and D. Anderson, Theoretical basis of some empirical relations in seismology, *Bull. Seismol. Soc. Am.*, *65*, 1073–1095, 1975.

Kendall, M. G., and P. A. P. Moran, *Geometrical Probability*, 125 pp., Griffin, London, 1963.

King, G. C. P., The accommodation of large strains in the upper lithosphere of the Earth and other solids by self-similar fault systems, *Pure Appl. Geophys.*, *12*, 761–815, 1983.

Knott, S. D., A. Beach, P. J. Brockbank, J. L. Brown, J. E. McCallum, and A. I. Welbon, Spatial and mechanical controls on normal fault population, *J. Struct. Geol.*, *18*, 359–372, 1996.

Krantz, R. L., Microcracks in rocks: A review, *Tectonophysics*, *100*, 449–480, 1983.

Krantz, R. L., Multiple fault sets and three-dimensional strain: Theory and application, *J. Struct. Geol.*, *10*, 225–237, 1988.

Kulatilake, P. H. S. W., and T. H. Wu, Estimation of mean trace length discontinuities, *Rock Mech. Rock Eng.*, *17*, 215–232, 1984.

Laherrere, J., and D. Sornette, Stretched exponential distributions in nature and economy: Fat tails with characteristic scales, *Eur. Phys. J.*, *B2*, 525–539, 1998.

LaPointe, P. R., A method to characterise fracture density and connectivity through fractal geometry, *Int. J. Rock Mech. Min. Sci. Geomech. Abstr.*, *25*, 421–429, 1988.

LaPointe, P. R., and J. A. Hudson, Characterization and interpretation of rock mass joint patterns, *Spec. Pap. Geol. Soc. Am.*, *199*, 37 pp., 1985.

Laslett, G. M., Censoring and edge effects in areal and line transect sampling of rock joint traces, *Math. Geol.*, *14*, 125–140, 1982.

Lawn, B., *Fracture of Brittle Solids*, 2nd ed., Cambridge Univ. Press, New York, 1993.

Ledésert, B., J. Dubois, J. Velde, A. Meunier, A. Genter, and A. Badri, Geometrical and fractal analysis of a three-dimensional hydrothermal vein network in a fractured granite, *J. Volcanol. Geotherm. Res.*, *56*, 267–280, 1993a.

Ledésert, B., J. Dubois, A. Genter, and A. Meunier, Fractal analysis of fractures applied to Soulz-sous-forets hot dry rock geothermal program, *J. Volcanol. Geotherm. Res.*, *57*, 1–17, 1993b.

Lindsay, R. W., and D. A. Rothrock, Arctic sea ice leads from advanced very high resolution radiometer images, *J. Geophys. Res.*, *100*, 4533–4544, 1995.

Line, C. E. R., D. B. Snyder, and R. W. Hobbs, The sampling of fault populations in dolerite sills of central Sweden and implications for resolution of seismic data, *J. Struct. Geol.*, *19*, 687–701, 1997.

Lockner, D. A., and T. R. Madden, A multiple-crack model of brittle fracture, 1, Non-time-dependent simulations, *J. Geophys. Res.*, *96*, 19,623–19,643, 1991.

Lockner, D. A., D. E. Moore, and Z. Reches, Microcracks interaction leading to shear fracture, in *Rock Mechanics: Proceedings of the 33rd U.S. Symposium on Rock Mechanics*, edited by J. R. Tillerson and W. R. Wawersik, pp. 807–816, A. A. Balkema, Brookfield, Vt., 1992.

Lovejoy, S., and D. Schertzer, Multifractal analysis techniques and the rain and cloud fields from 10^{-3} to 10^{6} m, in *Non-Linear Variability in Geophysics*, edited by D. Schertzer and S. Lovejoy, pp. 111–144, Kluwer Acad., Norwell, Mass., 1991.

Main, I. G., Statistical physics, seismogenesis, and seismic hazard, *Rev. Geophys.*, *34*, 433–462, 1996.

Main, I. G., Apparent breaks in scaling in the earthquake cumulative frequency-magnitude distribution: Fact or artifact?, *Bull. Seismol. Soc. Am.*, *90*, 86–97, 2000.

Main, I. G., and P. W. Burton, Information theory and the earthquake frequency magnitude distribution, *Bull. Seismol. Soc. Am.*, *74*, 1409–1426, 1984.

Main, I. G., T. Leonard, O. Papasouliotis, C. G. Hatton, and P. G. Meredith, One slope or two? Detecting statistically significant breaks of slope in geophysical data, with application to fracture scaling relationships, *Geophys. Res. Lett.*, *26*, 2801–2804, 1999.

Mandelbrot, B. B., *The Fractal Geometry of Nature*, W. H. Freeman, New York, 1982.

Marrett, R., Aggregate properties of fracture populations, *J. Struct. Geol.*, *18*, 169–178, 1996.

Marrett, R., and R. Allmendinger, Estimates of strain due to brittle faulting: Sampling of fault populations, *J. Struct. Geol.*, *13*, 735–738, 1991.

Martinod, J., and P. Davy, Periodic instabilities during compression or extension of the lithosphere, 1, Deformation modes from an analytical perturbation method, *J. Geophys. Res.*, *97*, 1999–2024, 1992.

Martinod, J., and P. Davy, Periodic instabilities during compression of the lithosphere, 2, Experiments, *J. Geophys. Res.*, *99*, 12,057–12,069, 1994.

Matsumoto, N., K. Yomogida, and S. Honda, Fractal analysis of fault systems in Japan and the Philippines, *Geophys. Res. Lett.*, *19*, 357–360, 1992.

Merceron, T., and B. Velde, Application of Cantor's method for fractal analysis of fractures in the Toyoha Mine, Hokkaido, Japan, *J. Geophys. Res.*, *96*, 16,641–16,650, 1991.

Moore, D. E., and D. A. Lockner, The role of microcracking in shear fracture propagation, in granite, *J. Struct. Geol.*, *17*, 95–114, 1995.

Needham, T., G. Yielding, and R. Fox, Fault population de-

scription and prediction using examples from the offshore U.K., *J. Struct. Geol.*, *18*, 155–167, 1996.
Nicol, A., J. J. Walsh, and J. Watterson, Fault size distributions—Are they really power-law?, *J. Struct. Geol.*, *18*, 191–197, 1996.
Nielsen, S., L. Knoppof, and A. Tarantola, Model of earthquake recurrence: Role of elastic wave radiation, relaxation of friction, and inhomogeneity, *J. Geophys. Res.*, *100*, 12,423–12,430, 1995.
Nur, A., The origin of tensile fracture lineaments, *J. Struct. Geol.*, *4*, 31–40, 1982.
Odling, N. E., Network properties of a two-dimensional fracture pattern, *Pure Appl. Geophys.*, *138*, 95–114, 1992.
Odling, N. E., Scaling and connectivity of joint systems in sandstones from western Norway, *J. Struct. Geol.*, *19*, 1257–1271, 1997.
Odling, N. E., et al., Variations in fracture system geometry and their implications for fluid flow in fractured hydrocarbon reservoirs, *Pet. Geosci.*, *5*, 373–384, 1999.
Okubo, P. G., and K. Aki, Fractal geometry in the San Andreas fault system, *J. Geophys. Res.*, *92*, 345–355, 1987.
Ouillon, G., C. Castaing, and D. Sornette, Hierarchical geometry of faulting, *J. Geophys. Res.*, *101*, 5477–5487, 1996.
Pacheco, J. F., C. H. Scholz, and L. R. Sikes, Change in the frequency-size relationship from small to large earthquakes, *Nature*, *355*, 71–73, 1992.
Pahl, P. J., Estimating the mean length of discontinuity traces, *Int. J. Rock Mech. Min. Sci. Geomech. Abstr.*, *18*, 221–228, 1981.
Peacock, D. C. P., and D. J. Sanderson, Displacements, segment linkage and relay ramps in normal fault zones, *J. Struct. Geol.*, *13*, 721–733, 1991.
Pickering, G., J. M. Bull, and D. J. Sanderson, Sampling power-law distributions, *Tectonophysics*, *248*, 1–20, 1995.
Pickering, G., J. M. Bull, and D. J. Sanderson, Scaling of fault displacements and implications for the estimation of subseismic strain, in *Modern Development in Structural Geology: Interpretation, Validation and Modelling*, edited by P. G. Buchanan and D. A. Nieuwland, *Geol. Soc. Spec. Publ.*, *99*, 11–26, 1996.
Pickering, G., D. C. P. Peacock, D. J. Sanderson, and J. M. Bull, Modeling tip zones to predict the throw and length characteristics of faults, *Am. Assoc. Pet. Geol. Bull.*, *81*, 82–99, 1997.
Piggott, A. R., Fractal relations for the diameter and trace length of disc-shaped fractures, *J. Geophys. Res.*, *102*, 18,121–18,125, 1997.
Poliakov, A. N. B., and H. J. Herrmann, Self-organized criticality of plastic shear bands in rocks, *Geophys. Res. Lett.*, *21*, 2143–2146, 1994.
Poliakov, A. N. B., H. Herrmann, Y. Y. Podladchikov, and S. Roux, Fractal plastic shear bands, *Fractals*, *2*, 567–581, 1994.
Priest, S. D., and J. A. Hudson, Discontinuity spacing in rock, *Int. J. Rock Mech. Min. Sci. Geomech. Abstr.*, *13*, 135–148, 1976.
Priest, S. D., and J. A. Hudson, Estimation of discontinuity spacing and trace length using scanline surveys, *Int. J. Rock Mech. Min. Sci. Geomech. Abstr.*, *18*, 183–197, 1981.
Pyrak-Nolte, L. J., C. D. Montemagno, and D. D. Nolte, Volumetric imaging of aperture distributions in connected fracture networks, *Geophys. Res. Lett.*, *24*, 2343–2346, 1997.
Reches, Z., Network of shear faults in the field and in experiment, in *Fragmentation, Form and Flow in Fractured Media*, edited by R. Englman and Z. Jaeger, *Ann. Isr. Phys. Soc.*, *8*, 42–51, 1986.
Renshaw, C. E., Computationally efficient models for the growth of large fracture systems, in *Fracture of Rock*, edited by M. H. Aliabadi, pp. 83–124, Comput. Mech., Southampton, England, 1999.
Renshaw, C. E., and J. C. Park, Effect of mechanical interactions on the scaling of fracture length and aperture, *Nature*, *386*, 482–484, 1997.
Renshaw, C. E., and D. D. Pollard, Numerical simulations of fracture set formation: A fracture mechanics model consistent with experimental observations, *J. Geophys. Res.*, *99*, 9359–9372, 1994.
Reuschlé, T., Fracture in heterogeneous medium: A network approach, *Terra Nova*, *4*, 591–597, 1992.
Ricard, Y., and C. Froidevaux, Stretching instabilities and lithospheric boudinage, *J. Geophys. Res.*, *91*, 8314–8324, 1986.
Rives, T., M. Razack, J. P. Petit, and K. D. Rawnsley, Joint spacing: Analogue and numerical simulations, *J. Struct. Geol.*, *14*, 925–937, 1992.
Rouleau, A., and J. E. Gale, Statistical characterization of the fracture system in the Stripa granite, Sweden, *Int. J. Rock Mech. Min. Sci. Geomech. Abstr.*, *22*, 353–367, 1985.
Sanderson, D. J., S. Roberts, and P. Gumiel, A fractal relationship between vein thickness and gold grade in drill core from La Codosera, Spain, *Econ. Geol.*, *89*, 168–173, 1994.
Schlische, R. W., S. S. Young, R. V. Ackermann, and A. Gupta, Geometry and scaling of a population of very small rift-related normal faults, *Geology*, *24*, 683–686, 1996.
Schmittbuhl, J., and S. Roux, The influence of internal stresses on the fracture of heterogeneous media, *Model. Simul. Mater. Sci. Eng.*, *2*, 21–52, 1994.
Scholz, C. H., *The Mechanics of Earthquakes and Faulting*, 439 pp., Cambridge Univ. Press, New York, 1990.
Scholz, C. H., Earthquake and fault populations and the calculation of brittle strain, *Geowissenschaften*, *15*, 124–130, 1997.
Scholz, C. H., and P. Cowie, Determination of total strain from faulting using slip measurements, *Nature*, *346*, 837–838, 1990.
Scholz, C. H., N. H. Dawers, J. Z. Yu, M. H. Anders, and P. A. Cowie, Fault growth and fault scaling laws: Preliminary results, *J. Geophys. Res.*, *98*, 21,951–21,961, 1993.
Scott, R. B., and M. Castellanos, Stratigraphic and structural relations of the volcanic rock in drill holes USW GU-3 and USW G-3, Yucca Mountain, Nevada, *U.S. Geol. Surv. Open File Rep.*, *84-491*, 127 pp., 1984.
Segall, P., and D. D. Pollard, Joint formation in granitic rock of the Sierra Nevada, *Geol. Soc. Am. Bull.*, *94*, 563–575, 1983.
Simon, J. L., L. E. Arlegui, C. L. Liesa, and A. Maestro, Stress perturbations registered by jointing near strike-slip, normal, and reverse faults: Examples from the Ebro Basin, Spain, *J. Geophys. Res.*, *104*, 15,141–15,153, 1999.
Snow, D. T., The frequency and apertures of fractures in rock, *Int. J. Rock Mech. Min. Sci.*, *7*, 25–40, 1970.
Sornette, A., P. Davy, and D. Sornette, Fault growth in brittle-ductile experiments and the mechanics of continental collisions, *J. Geophys. Res.*, *98*, 12,111–12,139, 1993.
Sornette, D., and P. Davy, Fault growth model and the universal fault length distribution, *Geophys. Res. Lett.*, *18*, 1079–1081, 1991.
Sornette, D., and A. Sornette, General theory of the modified Gutenberg-Richter law for large seismic moments, *Bull. Seismol. Soc. Am.*, *89*, 1121–1130, 1999.
Stauffer, D., and A. Aharony, *Introduction to Percolation Theory*, Taylor and Francis, Philadelphia, Pa., 1994.
Steen, Ø., and A. Andresen, Effects of lithology on geometry and scaling of small faults in Triassic sandstones, east Greenland, *J. Struct. Geol.*, *21*, 1351–1368, 1999.
Stewart, J. H., Geology of Nevada, *Spec. Publ. Nev. Bur. Mines Geol.*, *4*, 136 pp., 1980.
Stone, D., Sub-surface fracture maps predicted from borehole

data: An example from the Eye-Dashwa pluton, Atikokan, Canada, *Int. J. Rock Mech. Min. Sci. Geomech. Abstr.*, *21*, 183–194, 1984.

Triep, E. G., and L. R. Sykes, Frequency of occurrence of moderate to great earthquakes in intracontinental regions: Implications for changes in stress, earthquake prediction, and hazards assessment, *J. Geophys. Res.*, *102*, 9923–9948, 1997.

Trugdill, B., and J. Cartwright, Relay ramp forms and normal fault linkages, Canyonlands National Park, Utah, *Geol. Soc. Am. Bull.*, *106*, 1143–1157, 1994.

Turcotte, D. L., A fractal model for crustal deformation, *Tectonophysics*, *132*, 261–269, 1986.

Turcotte, D. L., *Fractals and Chaos in Geology and Geophysics*, 222 pp., Cambridge Univ. Press, New York, 1992.

Vanneste, C., and D. Sornette, The dynamical thermal fuse model, *J. Phys. I*, *2*, 1621–1644, 1992.

Velde, B., J. Dubois, G. Touchard, and A. Badri, Fractal analysis of fractures in rocks: The Cantor's dust method, *Tectonophysics*, *179*, 345–352, 1990.

Velde, B., J. Dubois, D. Moore, and G. Touchard, Fractal patterns of fractures in granites, *Earth Planet. Sci. Lett.*, *104*, 25–35, 1991.

Velde, B., D. Moore, A. Badri, and B. Ledésert, Fractal and length analysis of fractures during brittle to ductile changes, *J. Geophys. Res.*, *98*, 11,935–11,940, 1993.

Vendeville, B., P. R. Cobbold, P. Davy, J. P. Brun, and P. Choukroune, Physical models of extensional tectonics at various scales, in *Continental Extension Tectonics*, edited by M. P. Coward, J. F. Dewey, and P. L. Hancock, *Geol. Soc. London Spec. Publ.*, *28*, 95–107, 1987.

Vermilye, J. M., and C. H. Scholz, Relation between vein length and aperture, *J. Struct. Geol.*, *17*, 423–434, 1995.

Vicsek, T., *Fractal Growth Phenomena*, 488 pp., World Sci., River Edge, N. J., 1992.

Vignes-Adler, M., A. Le Page, and P. M. Adler, Fractal analysis of fracturing in two African regions, from satellite imagery to ground scale, *Tectonophysics*, *196*, 69–86, 1991.

Villaescusa, E., and E. T. Brown, Maximum likehood estimation of joint size from trace measurements, *Rock Mech. Rock Eng.*, *25*, 67–87, 1992.

Villemin, T., and C. Sunwoo, Distribution logarithmique self similaire des rejets et longueurs de failles: Exemple du bassin Houiller Lorrain, *C. R. Acad. Sci., Ser. II*, *305*, 1309–1312, 1987.

Volant, P., and J. R. Grasso, The finite extension of fractal geometry and power-law distribution of shallow earthquakes: A geomechanical effect, *J. Geophys. Res.*, *99*, 22,879–22,889, 1994.

Walmann, T., Dynamics and scaling properties of fractures in clay-like materials, Ph.D. thesis, Dep. of Phys., Univ. of Oslo, Oslo, 1998.

Walmann, T., A. Malthe Sørensen, J. Feder, T. Jøssang, and P. Meakin, Scaling relations for the lengths and widths of fractures, *Phys. Rev. Lett.*, *77*, 5393–5396, 1996.

Walsh, J. J., and J. Watterson, Analysis of the relationship between displacement and dimensions of faults, *J. Struct. Geol.*, *10*, 239–247, 1988.

Walsh, J. J., and J. Watterson, Fractal analysis of fracture pattern using the standard box-counting technique: Valid and invalid methodologies, *J. Struct. Geol.*, *15*, 1509–1512, 1993.

Walsh, J., J. J. Watterson, and G. Yielding, The importance of small-scale faulting in regional extension, *Nature*, *351*, 391–393, 1991.

Warburton, P. M., A stereological interpretation of joint traces data, *Int. J. Rock Mech. Min. Sci. Geomech. Abstr.*, *17*, 181–190, 1980.

Watterson, J., J. J. Walsh, P. A. Gillespie, and S. Easton, Scaling systematics of fault sizes on a large range fault map, *J. Struct. Geol.*, *18*, 199–214, 1996.

Westaway, R., Quantitative analysis of population of small faults, *J. Struct. Geol.*, *16*, 1259–1273, 1994.

Wong, T. F., J. T. Fredrich, and G. D. Gwanmesia, Crack aperture statistics and pore space fractal geometry of Westerly granite and Rutland quartzite: Implications for an elastic contact model of rock compressibility, *J. Geophys. Res.*, *94*, 10,267–10,278, 1989.

Wu, H., and D. D. Pollard, An experimental study of the relationship between joint spacing and layer thickness, *J. Struct. Geol.*, *17*, 887–905, 1995.

Yeomans, J. M., *Statistical Mechanics of Phase Transitions*, Clarendon, Oxford, England, 1992.

Yielding, G., J. J. Walsh, and J. Watterson, The prediction of small scale faulting in reservoirs, *First Break*, *10*, 449–460, 1992.

Yielding, G., T. Needham, and H. Jones, Sampling of fault population using sub-surface data: A review, *J. Struct. Geol.*, *18*, 135–146, 1996.

Zuber, M. T., E. M. Parmentier, and R. C. Fletcher, Extension of continental lithosphere: A model for two scales of basin and ranges deformation, *J. Geophys. Res.*, *91*, 4826–4838, 1986.

B. Berkowitz, Department of Environmental Sciences and Energy Research, Weizmann Institute of Science, Rehovot 76100, Israel.

E. Bonnet, Nansen Center, Edvard Griegsvei 3A, N-5059 Bergen, Norway.

O. Bour and P. Davy, Geosciences Rennes, UPR 4661 Campus de Beaulieu, Université Rennes, 35042 Rennes Cedex, France.

P. Cowie and I. Main, Department of Geology and Geophysics, University of Edinburgh, King's Buildings, West Mains Road, Edinburgh EH9 3JW, Scotland, UK.

N. E. Odling, Rock Deformation Research Group, School of Earth Sciences, University of Leeds, LS2 9JT Leeds, England, UK. (n.odling@rdr.leeds.ac.uk)